CHAPTER 1

Principle, Purpose and Pitfalls of Field-cycling NMR Relaxometry

RAINER KIMMICH

University of Ulm, 89081 Ulm, Germany
Email: rainer.kimmich@uni-ulm.de

The objective of this book is to introduce the reader to the theory of NMR relaxometry, to the field-cycling technique in all its variants, to instrumental aspects, to model concepts of molecular dynamics and to the large variety of applications including their future perspectives. This first chapter is intended to outline essential principles and to draw attention to key issues that sometimes lead to misunderstandings or even misinterpretations. For more comprehensive discussions of certain application aspects of the technique, we will frequently refer to subsequent, more specific chapters.

1.1 Revelation and Analytical Representation of Molecular Fluctuations

The primary purpose of field-cycling NMR relaxometry is to study molecular dynamics in condensed materials and systems. Nuclear magnetic relaxation is examined as a function of the angular Larmor frequency $\omega = 2\pi\nu = |\gamma|B_0$, where γ is the gyromagnetic ratio of the experimentally resonant nuclei and B_0 is the external magnetic flux density quantizing the spin states. The phenomenon of interest is normally the frequency dependence

New Developments in NMR No. 18
Field-cycling NMR Relaxometry: Instrumentation, Model Theories and Applications
Edited by Rainer Kimmich

Published by the Royal Society of Chemistry, www.rsc.org

(or 'dispersion') of spin–lattice relaxation with the time constant $T_1 = T_1(\omega)$ or the rate $1/T_1 \equiv R_1 = R_1(\omega)$.

From the theoretical point of view, the technique centres around one of the most fundamental principles of the statistical physics of stationary random processes, namely the Wiener/Khinchine theorem:

$$\mathcal{J}(\omega_k) = \int_{-\infty}^{+\infty} \mathcal{G}(\tau) \mathrm{e}^{-i\omega_k \tau} \mathrm{d}\tau \tag{1.1}$$

applied to molecular dynamics. The spectral density $\mathcal{J}(\omega_k)$ at the angular frequency ω_k is given as the Fourier transform of the autocorrelation

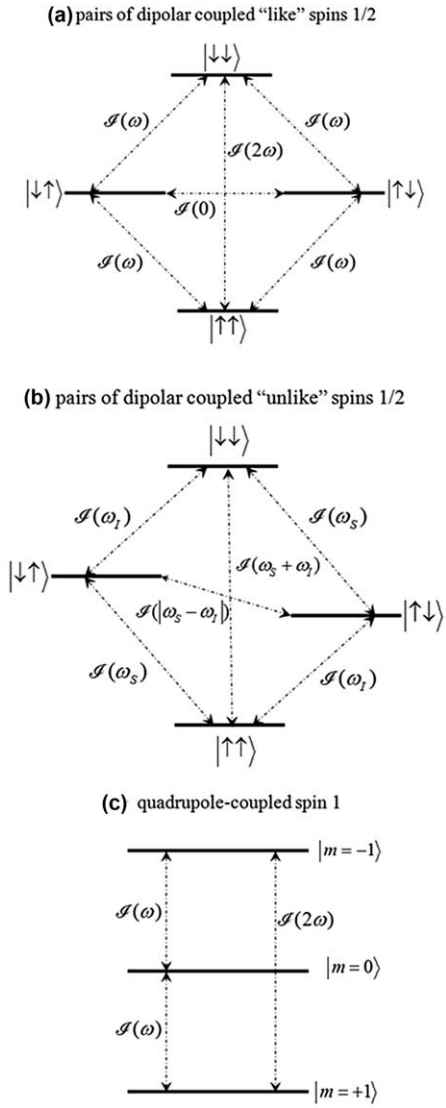

function $\mathcal{G}(\tau)$, where τ is the time interval conjugate to ω_k. The Wiener/Khinchine theorem links the key information carriers of molecular dynamics, $\mathcal{G}(\tau)$ and $\mathcal{J}(\omega_k)$, while the experimental access to these functions is provided by field-cycling NMR relaxometry in an unmatched way.

Later, we will identify ω_k with angular transition frequencies in spin systems as far as they are relevant in the present context. Spin–lattice relaxation of coupled 'like' spins can be traced back to angular single- and double-quantum transition frequencies $\omega_k = k\omega$, where $k = 1$, 2 and $\omega = |\gamma|B_0$ is the angular Larmor frequency of the spins. In the case of coupled 'unlike' spins with spin quantum numbers I, S, zero-quantum transitions also matter. In this case, the relevant angular transition frequencies are $\omega_0 = |\omega_S - \omega_I|$, $\omega_1 = \omega_1$ and $\omega_2 = \omega_S + \omega_I$, where $\omega_I = |\gamma_I|B_0$ is the angular Larmor frequency of the resonant spins I, and $\omega_S = |\gamma_S|B_0$ that of the coupling partners that are off-resonant in the experiment. For an illustration, see Figure 1.1.

The meaning of the functions $\mathcal{G}(\tau)$ and $\mathcal{J}(\omega_k)$ in terms of parameters of molecular dynamics will be specified below in more detail. Generally, a function $F(t)$ is defined characterizing molecular orientations and neighbour distances in terms of thermally fluctuating spherical coordinates $r(t)$, $\varphi(t)$, $\vartheta(t)$ [see Figure 1.2 and eqn (1.10) for fluctuations of dipolar couplings]. The autocorrelation function thereof is defined by

$$\mathcal{G}(\tau) \equiv \frac{\langle F(t)F^*(t+\tau)\rangle}{\langle |F(t)|^2\rangle} \tag{1.2}$$

Figure 1.1 Zeeman energy levels of spin systems in a quantizing field $\vec{B}_0$ (assumed to point upwards). The double arrows between the levels indicate the (allowed) zero-, single-, and double-quantum transitions relevant for spin relaxation. The spectral densities $\mathcal{J}(\omega_k)$ of the fluctuations inducing these transitions are indicated. In the schemes, all gyromagnetic ratios are assumed to be positive. (a) Dipolar coupled *'like' spin pairs* with quantum numbers $I = \frac{1}{2}$, $S = \frac{1}{2}$, magnetic quantum numbers m_I, m_S and a common gyromagnetic ratio γ. The spin eigenstates are symbolized by kets $|\uparrow\uparrow\rangle$, $|\uparrow\downarrow\rangle$, $|\downarrow\uparrow\rangle$ and $|\downarrow\downarrow\rangle$ for the diverse combinations of spin-up and spin-down states relative to the vector $\vec{B}_0$. The Zeeman eigenenergies are $E_{m_I,m_S} = -(m_I + m_S)\hbar\omega$, where $\omega = \gamma B_0$ is the angular Larmor frequency. The angular transition frequencies are $\omega_k = k\omega$ for zero- ($k = 0$), single- ($k = 1$) and double- ($k = 2$) quantum transitions. Typical examples are protons in organic materials. (b) Pairs of dipolar coupled *'unlike' spins* $\frac{1}{2}$ having different gyromagnetic ratios $\gamma_I \neq \gamma_S$ and Larmor frequencies $\omega_I = \gamma_I B_0$ and $\omega_S = \gamma_S B_0$. The Zeeman eigenenergies are $E_{m_I,m_S} = -\gamma_I\hbar m_I B_0 - \gamma_S\hbar m_S B_0$. The angular transition frequencies are $\omega_k = |\Delta E_k|/\hbar$ for zero- ($\omega_0 = |\omega_S - \omega_I|$), single- ($\omega_1 = \omega_I$) and double- ($\omega_2 = \omega_S + \omega_I$) quantum transitions. Typical examples are protons with spins I coupled to unpaired electrons with spin S. (c) (Single) spins 1 subjected to quadrupole interaction in the high-field limit. Quadrupolar coupled spin-1 particles have three Zeeman eigenstates with the kets $|m = 1\rangle$, $|m = 0\rangle$ and $|m = -1\rangle$ and energies $E_m = -m\hbar\omega$. The angular Larmor frequency is $\omega = \gamma B_0$ as before. The angular transition frequencies are $\omega_k = |\Delta E_k|/\hbar = k\omega$ for single- ($k = 1$) and double- ($k = 2$) quantum transitions. Typical examples are deuterons.

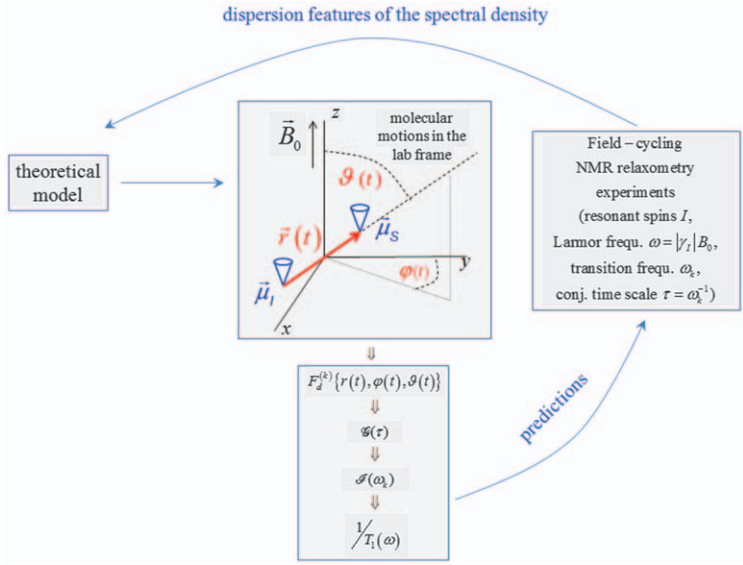

Figure 1.2 Schematic representation of the interrelations of molecular motions, field-cycling NMR relaxometry experiments and theoretical model concepts. Dipolar couplings between two dipoles with the vector operators $\vec{\mu}_I = \gamma_I \hbar \vec{I}$ and $\vec{\mu}_S = \gamma_S \hbar \vec{S}$ depend on the inter-dipole vector $\vec{r}$. If $\vec{\mu}_I$ and $\vec{\mu}_S$ are identical, one speaks of 'like' spins. The cones symbolize precession about the external flux density $\vec{B}_0$. $\vec{r}$ can be expressed in spherical coordinates $r(t)$, $\phi(t)$, $\vartheta(t)$ fluctuating as a consequence of molecular dynamics. For dipolar couplings, the autocorrelation function $\mathcal{G}(\tau)$ is formed on the basis of the functions $F_d^{(k)}\{r(t), \varphi(t), \vartheta(t)\}$ [see eqn (1.10)]. Note that the functions $F_d^{(k)}$ depend on the *absolute time* t whereas the autocorrelation function varies with the time *interval* τ. The spectral densities $\mathcal{J}(\omega_k)$ are Fourier transforms of $\mathcal{G}(\tau)$ for the angular frequencies ω_k. They determine the spin–lattice relaxation rate as a linear combination for all allowed angular transition frequencies ω_k in the spin system under consideration. Predictions based on a theoretical model can be compared with experimental field-cycling NMR relaxometry data. The other way round, dispersion features of the spectral density deduced from experimental data can be taken as conditions to be fulfilled by dynamic models in question.

in its 'normalized' or 'reduced' form with the initial value $\mathcal{G}(\tau = 0) = 1$. The asterisk indicates that the conjugate complex since the function $F(t)$ may be complex[†]. The angular brackets indicate averages for ensembles of molecules.

The definition eqn (1.2) implies an important feature of molecular fluctuations at thermal equilibrium, namely *stationarity*. That is, the autocorrelation function depends on the interval τ, but does not depend

[†]Under the conditions relevant here, both functions, $\mathcal{G}(\tau)$ and $\mathcal{J}(\omega_k)$, are mandatorily *real* as required for observables.

on the absolute time t. We can therefore set $t = 0$ without loss of generality. Eqn (1.2) can thus be rewritten in the usual form as[‡]

$$\mathcal{G}(\tau) = \frac{\langle F(0)F^*(\tau)\rangle}{\langle |F(0)|^2\rangle} \tag{1.3}$$

A further important property of stochastic processes is the *invariance upon time reversal*. The autocorrelation function is not a matter of the question of which of the two times under consideration is before or after. That is,

$$\mathcal{G}(\tau) = \mathcal{G}(-\tau) \tag{1.4}$$

The time scale of correlation functions is characterized by the *correlation time*:

$$\tau_c = \frac{1}{1 - \mathcal{G}(\infty)} \int_0^\infty [\mathcal{G}(\tau) - \mathcal{G}(\infty)] \mathrm{d}\tau \tag{1.5}$$

A simple (but not necessarily realistic) example of an autocorrelation functions is the monoexponential decay:

$$\mathcal{G}(\tau) = \exp\left(-\frac{|\tau|}{\tau_c}\right) \tag{1.6}$$

which is Fourier conjugate to the Lorentzian spectral density:

$$\mathcal{J}(\omega_k) = \frac{2\tau_c}{1 + \omega_k^2 \tau_c^2} \tag{1.7}$$

Figure 1.3 shows a graphical representation of eqn (1.7). Note that here and in general it is important not to forget the magnitude bars in the expression for the autocorrelation function in order to avoid conflicts with the Wiener/Khinchine theorem eqn (1.1). The magnitude bars so to speak warrant the time-reversal invariance condition eqn (1.4).[§]

1.1.1 From Molecular Motions to Spin–Lattice Relaxation

Figure 1.2 shows a scheme of how experimental field-cycling NMR relaxometry results are interrelated with models for molecular dynamics. From empirical data for the spin–lattice relaxation dispersion, conclusions can be drawn concerning spectral densities $\mathcal{J}(\omega_k)$, whereas – the other way round – theoretical model treatments permit one to predict features of autocorrelation functions $\mathcal{G}(\tau)$ and, on this basis, what dispersion features are to be expected in experiments. Prior to any detailed data analysis, the time scale of molecular dynamics can directly be estimated from the dispersion range. For instance, if a finite dispersion slope is observed down to the lower

[‡]Note the strict distinction between absolute time t and time interval τ here and in the following.
[§]As an introduction into the statistical physics of stochastic processes in general and the Wiener/Khinchine theorem in particular, the monograph by Heer[1] can be recommended, for instance.

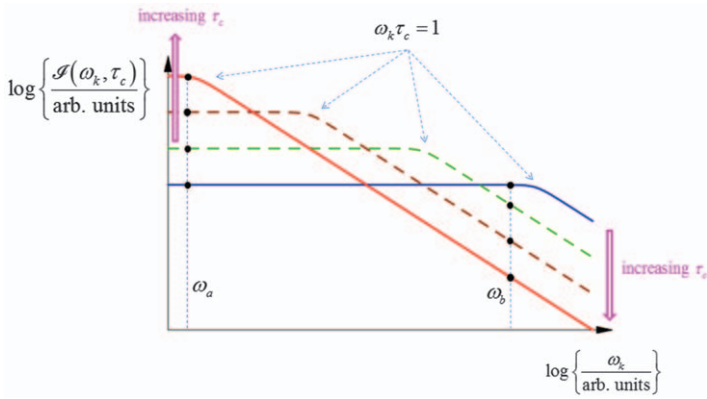

Figure 1.3 Graphical representation of a Lorentzian spectral density, eqn (1.7), as the Fourier transform of monoexponential autocorrelation functions, eqn (1.6), for different values of the correlation time τ_c. The crossover from the plateau $\mathcal{J}(\omega_k\tau_c \ll 1) \approx 2\tau_c$ at low angular frequencies to the limit $\mathcal{J}(\omega_k\tau_c \gg 1) \approx 2/(\omega_k^2\tau_c)$ at high angular frequencies occurs around the positions $\omega_k = \tau_c^{-1}$. Note that for $\omega_k < \tau_c^{-1}$, the spectral density $\mathcal{J}(\omega_k)$ *increases* with *increasing* values of τ_c and decreases in the opposite case $\omega_k > \tau_c^{-1}$. This is exemplified by the vertical lines and the dots at two angular frequencies complying with the respective conditions $\omega_a < \tau_c^{-1}$ and $\omega_b > \tau_c^{-1}$ in the frame of consideration here. Qualitatively, this behaviour applies generally to all stochastic processes irrespective of the actual shape of the autocorrelation function. With respect to field-cycling NMR relaxometry, this means that spin–lattice relaxation rates $1/T_1$ *increase* with longer τ_c values (*i.e.* slower fluctuations) for $\omega_k\tau_c < 1$ whereas they *decrease* for $\omega_k\tau_c > 1$.

end of the available frequency window, one *knows* that correlations exist longer than the inverse angular frequency ω_κ of the spin transition leading in that magnetic-field regime. A more specific discussion of this point follows in Section 1.1.2.

Most applications of field-cycling NMR relaxometry refer to scenarios where the standard formalism for nuclear spin relaxation applies. It is referred to as BWR (Bloch–Wangsness–Redfield) theory. The principle is as follows: molecular dynamics, *i.e.* rotational and translational Brownian motions, cause fluctuations of spin interactions, which in turn induce spin transitions. In the present context, dipole–dipole couplings and/or quadrupole interactions with molecular electric field gradients are of particular importance depending on the particle species under consideration. Spin interactions are treated as perturbations of the (much larger) Zeeman interaction with the external magnetic flux density B_0. Starting with a state of the spin ensemble initially at non-equilibrium, the fluctuating perturbations will induce spin transitions causing the evolution towards thermal equilibrium[¶].

[¶]As an example of non-Brownian fluctuations, quantum-mechanical tunneling will be discussed in Chapter 16.

1.1.1.1 Fluctuating Dipolar Couplings

The Hamiltonian of dipole–dipole couplings among a spin pair can be analysed in terms of linear combinations of products of spin operator expressions $\mathcal{O}_d^{(k)}$ and spatial functions $F_d^{(k)}(r, \varphi, \vartheta)$:

$$\mathcal{H}_d = f_d \sum_{k=-2}^{2} F_d^{(k)} \mathcal{O}_d^{(k)} \tag{1.8}$$

where

$$f_d = \frac{\mu_0}{4\pi} \hbar^2 \gamma_I \gamma_S \tag{1.9}$$

is a constant characteristic for the coupled spin pairs (μ_0, magnetic field constant; $\hbar$, Planck's constant divided by 2π; γ_I and γ_S, gyromagnetic ratios of the coupled dipoles with spin quantum numbers I and S, respectively). The functions $F_d^{(k)}(r, \varphi, \vartheta)$ depend on the (fluctuating) spherical coordinates r, φ, ϑ of the distance vector (see Figure 1.2). They are special versions of the function F in eqn (1.2) for dipolar couplings. These functions characterize the position- and orientation-dependent strength of dipolar couplings and are related to second-degree spherical harmonics according to

$$\begin{aligned}
F_d^{(0)}(r, \vartheta) &= F_d^{(0)*}(r, \vartheta) = r^{-3}(1 - 3\cos^2\vartheta) = -\sqrt{\frac{16\pi}{5}} \frac{1}{r^3} Y_{2,0}(\vartheta) \\
F_d^{(1)}(r, \varphi, \vartheta) &= F_d^{(-1)*}(r, \varphi, \vartheta) = r^{-3}(\sin\vartheta\cos\vartheta\, e^{-i\varphi}) = \sqrt{\frac{8\pi}{15}} \frac{1}{r^3} Y_{2,-1}(\varphi, \vartheta) \\
&= -\sqrt{\frac{8\pi}{15}} \frac{1}{r^3} Y^*_{2,1}(\varphi, \vartheta) \\
F_d^{(2)}(r, \varphi, \vartheta) &= F_d^{(-2)*}(r, \varphi, \vartheta) = r^{-3}(\sin^2\vartheta\, e^{-2i\varphi}) = \sqrt{\frac{32\pi}{15}} \frac{1}{r^3} Y_{2,-2}(\varphi, \vartheta) \\
&= \sqrt{\frac{32\pi}{15}} \frac{1}{r^3} Y^*_{2,2}(\varphi, \vartheta)
\end{aligned} \tag{1.10}$$

Based on fluctuations of the spherical coordinates r, φ, ϑ – and hence of the spatial functions $F_d^{(k)}(r, \varphi, \vartheta)$ – the respective spin operator terms $\mathcal{O}_d^{(k)}$ induce the allowed spin transitions indicated in Figure 1.1a or b.

The autocorrelation functions, eqn (1.3), for dipolar coupled spin pairs read

$$\mathcal{G}_k(\tau) = \frac{\left\langle F_d^{(k)}(0) F_d^{(k)*}(\tau) \right\rangle}{\left\langle |F_d^{(k)}(0)|^2 \right\rangle} \tag{1.11}$$

for the zero- ($k = 0$), single- ($k = \pm 1$) and double- ($k = \pm 2$) quantum spin transitions defined in Figure 1.1a and b. In the case of exclusively rotational

fluctuations, that is, for fixed (intramolecular) inter-dipole distances r, these expressions can be reduced to autocorrelation functions of second-degree spherical harmonics:

$$\mathscr{G}_k(\tau) \approx (-1)^k 4\pi \langle Y_{2,k}(0)\, Y_{2,-k}(\tau)\rangle \tag{1.12}$$

In disordered liquid systems where molecular reorientations are not restricted significantly by topological or steric constraints, the autocorrelation functions turn out to be independent of the order k, so that [compare eqn (1.75)]

$$\mathscr{G}_0(\tau) = \mathscr{G}_1(\tau) = \mathscr{G}_2(\tau) \equiv \mathscr{G}(\tau) \tag{1.13}$$

The corresponding spectral densities $\mathscr{I}(0)$, $\mathscr{I}(\omega)$ and $\mathscr{I}(2\omega)$ follow from eqn (1.1).

For dipolar coupled pairs of 'like' spins defined by identical gyromagnetic ratios, $\gamma_I = \gamma_S \equiv \gamma$, the BWR theory predicts the spin–lattice relaxation rate:

$$\frac{1}{T_1(\omega)} = \left(\frac{\mu_0}{4\pi}\right)^2 \frac{1}{5r^6} \gamma^4 \hbar^2 I(I+1)[\mathscr{I}(\omega) + 4\mathscr{I}(2\omega)] \tag{1.14}$$

where $\omega = |\gamma| B_0$ is the angular Larmor frequency.

The result for dipolar coupled pairs of 'unlike' spins with quantum numbers I (resonant), S (off-resonant) and gyromagnetic ratios $\gamma_I \neq \gamma_S$ is[‖]

$$\frac{1}{T_1(\omega_I)} = \left(\frac{\mu_0}{4\pi}\right)^2 \frac{1}{15r^6} \gamma_I^2 \gamma_S^2 \hbar^2 S(S+1)[\mathscr{I}(|\omega_I - \omega_S|) + 3\mathscr{I}(\omega_I) + 6\mathscr{I}(\omega_I + \omega_S)] \tag{1.15}$$

The angular Larmor frequencies for the two spin species are $\omega_I = |\gamma_I| B_0$ and $\omega_S = |\gamma_S| B_0$. Detailed descriptions, definitions and derivations of eqn (1.8)–(1.15) can be found in ref. 2–7, for instance.

Eqn (1.14) and (1.15) have been derived for a number of important premises that need to be commented upon:

1. The time scale of molecular fluctuations relevant for spin–lattice relaxation is limited by that of T_1. For slower motions, the BWR theory does not apply. This is expressed by the so-called *Redfield limit* $T_1 \gg \tau_c$ in terms of correlation times. Since T_1 is smallest at angular frequencies $\omega_k \leq \tau_c^{-1}$, *i.e.* where $\mathscr{I}(\omega_k)$ is largest (see Figure 1.3), the Redfield condition can also be expressed by $T_1 \gg \omega_k^{-1}$ with respect to the angular spin transition frequency ω_k dominating in eqn (1.14) or (1.15) under the experimental conditions.
2. In principle, these equations are valid for ensembles of isolated, *i.e.* independently fluctuating, *two-spin systems*. This assumption conflicts

[‖]If eqn (1.15) is to refer to spin–lattice relaxation of nuclear spins interacting with unpaired electrons, *scalar coupling*[2] as a further, additional mechanism for nuclear spin relaxation may also be relevant.

with the multi-spin composition of the materials of interest here. There are two reasons why the BWR theory nevertheless works: the dipolar Hamiltonian eqn (1.8) actually couples only two particles, so that the total dipolar Hamiltonian of a multi-spin system is composed of the sum of mutual two-spin interaction terms. A superposition of two-spin Hamiltonians complicates the treatment of the relaxation mechanism only if the fluctuations of two-spin couplings are correlated (as one would suspect for intramolecular multi-spin systems). *Correlation effects* are indeed perceptible in high-field, high-resolution NMR spectroscopy.[8,9] However, under the low-field conditions typical for field-cycling NMR relaxometry, such phenomena will scarcely influence the relaxation behaviour, even for practically rigid atomic arrangements such as methyl groups[10] or alkenes. Multi-spin systems can therefore be modelled as a set of independently fluctuating two-spin systems with an accuracy better than experimental errors.[11] Spin–lattice relaxation of dipolar coupled, multi-spin systems is thus represented by a sum of independent two-spin relaxation rates $1/T_1^{(i)}$:

$$\frac{1}{T_1} \approx \sum_i \frac{1}{T_1^{(i)}} \tag{1.16}$$

where the index i runs over all coupling partners with which a resonant spin interacts at a time. Some care should nevertheless be taken if field cycling is combined with high-field high-resolution NMR spectroscopy (see Chapters 15 and 21).

3. Eqn (1.14) and (1.15) hold for fixed dipole–dipole distances r, *i.e.* for *intramolecular* interactions fluctuating as a consequence of *rotational diffusion* of the spin-bearing molecule. However, dipolar couplings between spins located on different molecules may also be significant. This *intermolecular* dipolar interaction can give rise to a further relaxation contribution $1/T_1^{\text{inter}}$ in addition to the intramolecular rate $1/T_1^{\text{intra}}$:

$$\frac{1}{T_1} = \frac{1}{T_1^{\text{intra}}} + \frac{1}{T_1^{\text{inter}}} \tag{1.17}$$

The intermolecular relaxation rate is based on fluctuations of the intermolecular inter-dipole distance $\vec{r} = \vec{r}(t)$ due to translational diffusion and – to a minor extent – possibly also by rotational diffusion. For further details, see Sections 1.1.1.3 and 1.1.1.4.

4. The rotational and translational fluctuations referred to so far govern molecular dynamics in liquid-like systems. In solid-like materials such as immobilized macromolecules of synthetic or biological origin, the pervasive fluctuation process may rather be *vibrational dynamics* (see Chapter 9) and/or *diffusion of microstructural defects.*[5,14–16] A special case of this sort is collective vibration phenomena in field- or surface-ordered liquid crystals called *order director fluctuation*[17] (see Chapter 11 in this book and Chapter 6 in ref. 5).

5. The numerical factors weighting the spectral densities $\mathcal{J}(\omega_k)$ in eqn (1.14) and (1.15) at the allowed spin transition frequencies ω_k have been calculated for *unrestricted* rotational diffusion of the molecules on the time scale of spin–lattice relaxation (see Section 1.3.1). The averages $\langle|F_d^{(k)}|^2\rangle$ refer to the whole variation range of the angles defined in Figure 1.2, *i.e.* $0 \leq \varphi \leq 2\pi$ and $0 \leq \vartheta \leq \pi$, while r is assumed to be fixed. The results are related as follows:

$$\left\langle \left|F_d^{(0)}\right|^2 \right\rangle : \left\langle \left|F_d^{(1)}\right|^2 \right\rangle : \left\langle \left|F_d^{(2)}\right|^2 \right\rangle = \frac{12}{15}\left\langle \frac{1}{r^6} \right\rangle : \frac{2}{15}\left\langle \frac{1}{r^6} \right\rangle : \frac{8}{15}\left\langle \frac{1}{r^6} \right\rangle = 6:1:4 \tag{1.18}$$

The prerequisite of *unrestricted* molecular reorientations on the relaxation time scale will be violated in ordered systems such as liquid crystals or in materials implying strong reorientation constraints such as polymers.[5,18] Strictly, eqn (1.18) will then no longer apply. Effects on this basis can be demonstrated by comparing field-cycling NMR relaxometry data $1/T_1(\omega)$ with data measured with the aid of spin–lattice relaxation in the rotating frame, $1/T_{1\rho}(\omega_1)$. This rate refers to the angular frequency $\omega_1 = |\gamma|B_1$, where B_1 is the amplitude of the rotating radiofrequency (rf) flux density (see Chapter 7 and ref. 7). On the other hand, strongly constrained reorientation processes are often accompanied by superimposed faster components, reducing the effective spatial restrictions substantially. Taken as a whole, reorientations will then be largely unrestricted, and eqn (1.18) will be a good approach.

1.1.1.2 Fluctuating Quadrupole Interactions

The second type of spin interaction of major interest is the coupling of nuclear electric quadrupoles to electric field gradients produced by asymmetric charge distributions in molecules. Analogously to the dipolar Hamiltonian eqn (1.8), the Hamiltonian of a nucleus with a spin quantum number $I \geq 1$ and a quadrupole moment Q interacting with an effectively rotationally symmetric electric field gradient can be expressed by[7]

$$\mathcal{H}_q = f_q \sum_{k=-2}^{2} F_q^{(k)} \mathcal{O}_q^{(k)} \tag{1.19}$$

The constant $f_q = e^2qQ/[8I(2I-1)]$ characterizes the nuclear species and the strength of the electric field gradient in the molecule (e, positive elementary charge; $q = \Gamma_{33}/e$, largest field-gradient component divided by e). The operators $\mathcal{O}_d^{(k)}$ represent spin operator terms responsible for allowed spin transitions, *i.e.* single- and double-quantum transitions (see Figure 1.1c). The spatial functions $F_q^{(k)}(\vartheta)$ depend on the polar angle ϑ defined by the orientation of the quantizing field $\vec{B}_0$ relative to the principal axis system of the field-gradient tensor. Note that this definition deviates from that for

dipolar couplings, as illustrated in Figure 1.2. However, in both cases, the polar angle ϑ fluctuates as a consequence of rotational diffusion relative to the laboratory frame. Owing to the rotational symmetry of the electric field-gradient tensor anticipated here, the azimuth angle does not matter and can arbitrarily be set as $\varphi = 0$:

$$F_q^{(0)}(\vartheta) = (3\cos^2\vartheta - 1) = \sqrt{\frac{16\pi}{5}} Y_{2,0}(\vartheta)$$

$$F_q^{(1)}(\vartheta) = 3\sin\vartheta\cos\vartheta = \sqrt{\frac{24\pi}{5}} Y_{2,1}(\vartheta, \varphi = 0) \tag{1.20}$$

$$F_q^{(2)}(\vartheta) = \frac{3}{2}\sin^2\vartheta = \sqrt{\frac{24\pi}{5}} Y_{2,2}(\vartheta, \varphi = 0)$$

Of these expressions, the second and third are relevant for spin–lattice relaxation: The spin operators $\mathcal{O}_q^{(\pm 1)}$ and $\mathcal{O}_q^{(\pm 2)}$ produce the transitions illustrated in Figure 1.1c. Eqn (1.11)–(1.13) apply in an analogous way again. The spin–lattice relaxation rate of quadrupolar coupled spins 1 in rotationally symmetric electric field gradients is thus found to obey

$$\frac{1}{T_1(\omega)} = \frac{3}{80}\left(\frac{e^2qQ}{\hbar}\right)^2 [\mathcal{J}(\omega) + 4\mathcal{J}(2\omega)] \tag{1.21}$$

Detailed derivations can be found in ref. 2–7, for instance.

Two remarks referring mainly to deuterons ($I = 1$) may be appropriate in this context:

1. As in the dipolar coupling case, the Redfield limit requiring $T_1 \gg \omega^{-1}$ applies for the applicability of eqn (1.21).
2. Quadrupole couplings to electric field gradients in molecules are relatively strong, so that dipolar interactions from deuteron to deuteron or from resonant deuterons to protons or – at moderate concentrations – from resonant deuterons to electron paramagnetic centres are normally negligible. Deuteron spin–lattice relaxation therefore reflects *single*-spin – and hence *intramolecular* – phenomena.

1.1.1.3 Experimental Distinction of Intra- and Intermolecular Relaxation

In condensed matter consisting of multi-spin molecules, which is the case in practically all materials of interest here, we have a superposition of intramolecular and intermolecular spin–lattice relaxation rates as expressed by eqn (1.17). Intermolecular relaxation can refer to fluctuating couplings to both 'like' and 'unlike' dipoles located on different molecules. The latter interaction partners may also include electron paramagnetic ions or centres. An intra/inter distinction is important if, for instance, there are doubts

about whether relaxation in aqueous systems is governed by intramolecular proton–proton couplings or by intermolecular interactions with electron paramagnetic ions. Cases of this or similar sorts raise the question of how to distinguish and quantify the two contributions in experiments. There are diverse scenarios that will be discussed one by one.

1. The simplest situation arises if spin–lattice relaxation dispersion data for deuterons are available for comparison with proton data of the same chemical system. Eqn (1.16) for multi-spin interactions and eqn (1.17) for intermolecular contributions are insignificant in the deuteron case (provided that there is no excessive abundance of electron paramagnetic centres). Deuteron relaxation is therefore an intrinsically intramolecular and single-spin mechanism. Such a comparison has been exemplified in ref. 13, where it was shown that the low-frequency relaxation mechanism in water confined in silica porous glasses is of an exclusively intramolecular nature.
2. For proton resonance of *non-exchangeable* hydrogen atoms, intermolecular proton–proton couplings can be reduced by isotopic dilution, that is, by mixing perdeuterated and undeuterated homologues. The gyromagnetic ratio of deuterons is 6.5 times smaller than that of protons. The spin–lattice relaxation rate of protons that are dipolar coupled to deuterons will therefore be reduced by a factor of 42 relative to homonuclear proton systems [see the quadratic prefactor of eqn (1.15)]. In this way, the term $1/T_1^{\mathrm{intra}}$ in eqn (1.17) can be discriminated from $1/T_1^{\mathrm{inter}}$. This method has been exploited, *e.g.*, for studies of translational diffusion in polymers (see Section 1.1.1.4, Chapters 8 and 13 and ref. 12). Note that intermolecular couplings tend to fluctuate more slowly than the intramolecular counterpart. As a consequence, they will reveal themselves particularly at low frequencies, and can then even dominate.
3. If *exchangeable* hydrogen atoms are probed in the experiment – the simplest example of this sort is water – isotopic dilution in principle affects both intra- and intermolecular couplings. However, a closer analysis reveals that the effect in aqueous systems will be tendentially just the *opposite* of that discussed above. The isotope exchange after mixing light and heavy water will be complete after a few milliseconds at neutral pH (or pD). The distribution of protons and deuterons can then be assessed as follows: Let x be the fraction of H atoms. The fraction of D atoms is consequently $1-x$. We thus have the respective fractions x^2, $2x(1-x)$ and $(1-x)^2$ of H_2O, HDO and D_2O molecules. A fraction $x=1/4$, for instance, results in a distribution ratio of 1 : 6 : 9 for H_2O, HDO and D_2O molecules, which means six times more HDO molecules than H_2O. The proton spin–lattice relaxation rate of HD spin pairs is only a fraction of 1/42 of that of HH pairs as mentioned above. Proton–deuteron couplings can therefore be neglected for proton relaxation irrespective of the intra- or intermolecular cases, provided

that the proton fraction x is not too small**. It remains to compare the contributions of intramolecular couplings in the residual H_2O molecules with those of intermolecular interactions of *all* H nuclei in both HDO and H_2O molecules. In the example above, the intramolecular H–H contribution is reduced by a factor of $x^2 = 1/16$ relative to undeuterated water, and that of intermolecular H–H relaxation is diminished by a factor of $2x^2 + 2x(1-x) = 1/2$. The first term refers to the likelihood of a given water proton finding a proton coupling partner in an H_2O molecule in its vicinity and the second expression to that of facing a proton of an HDO molecule. That is, *intermolecular* H–H spin–lattice relaxation will dominate over the intramolecular H–H contribution. This holds in terms of numbers of available proton interaction partners, and is supported by the relaxation efficiency at sufficiently low frequencies. An exception to this rule is the RMTD process to be described in the next paragraph.

4. A third scenario concerning intra- and intermolecular spin–lattice relaxation has an amazing consequence: rotational fluctuations of intramolecular couplings can also be the *indirect* consequence of translational diffusion. A typical example is the migration of adsorbate molecules along adsorbent surfaces. Being adsorbed, the molecules will adopt a certain preferential orientation relative to the local surface topology (compare Figure 1.7c, Chapter 12 and ref. 5, 12 and 13). Starting from the adsorbed state, a molecule can be desorbed and – after an excursion to the bulk medium – be readsorbed. This process can occur repeatedly during the interval τ considered for the autocorrelation function decay. The crucial point is now that the initial orientation will be reconstituted at the final position subject to the degree of topological correlation between the initial and final adsorption sites. This process is referred to as reorientation mediated by translational displacements (RMTD)††. The startling feature of this recovery process is that it selectively applies to the correlation of *intramolecular* spin interactions, but not to *intermolecular* interactions. The initial correlation of intermolecular couplings among adsorbate molecules will soon and finally decay *via* translational diffusion, while intramolecular couplings are re-established subject to readsorption at sites with correlated surface orientations. This is the explanation of why intermolecular correlations do not influence the proton spin–lattice relaxation dispersion of water in porous glasses, as already mentioned. In that example, the intermolecular correlation will decay on a time scale on the order of 10^{-11} s near room temperature, whereas the intramolecular correlation can persist over 10^{-5} s or more.[13]

**For extremely small proton fractions – especially if relaxation rates are extrapolated to $x \to 0$ in concentration series – dipolar couplings between protons and deuterons will become significant despite their low efficiency.

††Other examples of RMTD in a more general sense are translational diffusion of molecules in ordered phases such as liquid crystals (see Chapter 11) and reptation of polymer segments under entanglement conditions (see Chapters 8 and 13).

Intramolecular relaxation will therefore dominate in the frequency window of the field-cycling technique. Further features of the RMTD process are discussed in Section 1.2.2.4.

1.1.1.4 Translational Diffusion Examined with the Aid of Intermolecular Spin–Lattice Relaxation

As reviewed in ref. 12, field-cycling NMR relaxometry can be employed for the determination of mean-square displacements by translational diffusion. The time scale ranges from nanoseconds to milliseconds and – if combined with conventional field-gradient NMR diffusometry[5,19,20] – up to seconds. The respective information is included in the intermolecular proton spin–lattice relaxation rate $1/T_1^{\text{inter}}(\omega)$. The primary problem to be solved is therefore to extract the intermolecular rate from data for the total rate $1/T_1(\omega)$ [eqn (1.17)]. This objective can be reached with the aid of isotopic dilution experiments already discussed in the previous Section for non-exchanging proton systems. Diminishing intermolecular dipolar couplings in this way permits one to evaluate the intramolecular contribution $1/T_1^{\text{intra}}(\omega)$ to proton spin–lattice relaxation. Subtracting this from the total rate eqn (1.17) provides the desired data sets for $1/T_1^{\text{inter}}(\omega)$ (compare Chapters 8 and 13).

The autocorrelation function for intermolecular dipolar couplings can be defined as

$$G_k^{\text{inter}}(\tau) = \left\langle F_d^{(k)}(\tau)\, F_d^{(k)*}(0) \right\rangle = c_k g_k^{\text{inter}}(\tau) \tag{1.22}$$

where $c_0 = 16\pi/5$, $c_1 = 8\pi/15$ and $c_2 = 32\pi/15$ [see eqn (1.10)]. The (unnormalized) autocorrelation functions to be evaluated for intermolecular dipolar couplings are

$$g_k^{\text{inter}}(\tau) = \frac{G_k(\tau)}{c_k} = (-1)^k \left\langle \frac{Y_{2,k}(\tau) Y^*_{2,k}(0)}{r^3(\tau) r^3(0)} \right\rangle \tag{1.23}$$

Under effectively isotropic conditions, we can equate

$$g_0^{\text{inter}}(\tau) = g_1^{\text{inter}}(\tau) = g_2^{\text{inter}}(\tau) \equiv g^{\text{inter}}(\tau) \tag{1.24}$$

in analogy with eqn (1.13). The spectral densities associated with $g_0^{\text{inter}}(\tau)$ are given by

$$\mathcal{J}_k^{\text{inter}}(\omega_k) = c_k \int_{-\infty}^{+\infty} g^{\text{inter}}(\tau) \mathrm{e}^{-i\omega_k \tau} \mathrm{d}\tau \tag{1.25}$$

Note that the symbols for the correlation function and the spectral density deviate from those used above for intramolecular interactions. This is due to the fact that these functions are not 'normalized' in the case of intermolecular couplings. The intermolecular proton–proton spin–lattice relaxation rate thus reads

$$\frac{1}{T_1^{\text{inter}}(\omega)} = \left(\frac{\mu_0}{4\pi}\right)^2 \frac{9}{8} \gamma^4 \hbar^2 \left[\mathcal{J}_1^{\text{inter}}(\omega) + \mathcal{J}_2^{\text{inter}}(2\omega) \right] \tag{1.26}$$

The version for protons ($I=\frac{1}{2}$) coupled to deuterons ($S=1$) is obtained by converting eqn (1.15) to

$$\frac{1}{T_1^{\text{inter}}(\omega_I)} = \left(\frac{\mu_0}{4\pi}\right)^2 \gamma_I^2 \gamma_S^2 \hbar^2 \left[\frac{1}{6} \mathcal{J}_0^{\text{inter}}(|\omega_I - \omega_S|) + 3\mathcal{J}_1^{\text{inter}}(\omega_I) + \frac{3}{2} \mathcal{J}_2^{\text{inter}}(\omega_I + \omega_S)\right] \tag{1.27}$$

At this point, we should add some comments on eqn (1.26) and (1.27) in addition to those on eqn (1.14) and (1.15):

1. The fluctuations of intermolecular dipolar couplings are not exclusively of a translational character, but will also depend on rotational diffusion to some minor extent if the interacting dipoles are not centred in the molecules (*eccentricity effect*).[12]
2. Having acquired data for intermolecular spin–lattice relaxation rates from isotopic dilution experiments as outlined above, the following question arises: how can we express translational diffusion properties in terms of these relaxation rates? This in particular refers to the second moment of the propagator, *i.e.* the mean-square displacement $\langle \rho^2 \rangle_{\text{rel}}$ of the diffusing particles relative to each other. In cases where disordered microstructural constraints substantially limit translational displacements, subdiffusive time dependences characterized by power laws can be expected:[5]

$$\langle \rho^2 \rangle_{\text{rel}} = \kappa \tau^{\alpha} \quad (0 < \alpha < 1) \tag{1.28}$$

where κ is a constant. Examples are random percolation networks in porous media[21] and segment diffusion in polymer melts (see Chapters 8 and 13). Provided that the exponent obeys $\alpha < 2/3$, the power law eqn (1.28) will be reflected by a conjugated power law for the dispersion of the intermolecular spin–lattice relaxation rate:[12]

$$\frac{1}{T_1^{\text{inter}}(\omega)} \propto \omega^{-\beta} \quad (0 < \beta < 1) \tag{1.29}$$

The relation between the conjugated exponents α and β is

$$\alpha = \frac{2}{3}(1 - \beta) \tag{1.30}$$

The restriction $\alpha < 2/3$ stipulates that both the time dependence of the mean-square displacement and the spin–lattice relaxation dispersion are power laws. In this case, one can directly relate the relative mean-square displacement and the spin–lattice relaxation time:

$$\underbrace{\left\langle \rho_{\text{rel}}^2\left(\tau = \frac{1}{\omega}\right)\right\rangle}_{\text{to be evaluated}} = \frac{1}{\pi}\left[\left(\frac{\mu_0}{4\pi}\right)^2 \frac{\sqrt{6}}{5} \gamma^4 n\right]^{-\frac{2}{3}} \left\{ \underbrace{\frac{\cos\left[\frac{\pi(1-\beta)}{2}\right]\Gamma(1-\beta)}{1+2^{2-\beta}} \frac{\omega}{T_1^{\text{inter}}(\omega)}}_{\text{to be measured}} \right\}^{\frac{2}{3}} \tag{1.31}$$

where $\Gamma(x)$ is Euler's gamma function and n is the number density of protons. The mean-square displacement of independently diffusing, free molecules relative to the laboratory frame is half of the relative mean-square displacement, *i.e.* $\langle\rho^2(\tau)\rangle = \frac{1}{2}\langle\rho^2_{\mathrm{rel}}(\tau)\rangle$.

1.1.2 What Time Scale of Autocorrelation Functions Do We Probe in NMR Relaxometry?

The conjugated variables of the Fourier transform between autocorrelation function and spectral density [eqn (1.1)] are time and the relevant angular spin transition frequency: $\tau \overset{\mathscr{F}}{\longleftrightarrow} \omega_k$. The parameter to be examined in NMR relaxometry is the angular Larmor frequency $\omega = |\gamma|B_0$ of the resonant spins. Spin–lattice relaxation of *like-spin or single-spin systems* results from single- and double-quantum transitions, as suggested by eqn (1.14) and (1.21), *i.e.* $\omega_1 = \omega$ and $\omega_2 = 2\omega$, respectively. For time-scale considerations, we may crudely equate Larmor and spin transition frequencies: $\omega \approx \omega_{k=1,2}$. The time interval after which the autocorrelation function is probed can thus be estimated as

$$\tau \approx \omega^{-1} \tag{1.32}$$

In the case of 'unlike' spins [see eqn (1.15) and (1.27)], the situation is more complicated since two different Larmor frequencies count, $\omega_I = |\gamma_I|B_0$ and $\omega_S = |\gamma_S|B_0$. A typical example is coupled pairs of protons (spin I) and unpaired electrons (spin S). Since $\omega_S \approx 662\omega_I$, we can approximate $\mathscr{J}(|\omega_I - \omega_S|) \approx \mathscr{J}(|\omega_I + \omega_S|) \approx \mathscr{J}(\omega_S)$. The question is then which of the two spectral densities $\mathscr{J}(\omega_I)$ and $\mathscr{J}(\omega_S)$ dominates spin–lattice relaxation of the I spins at the measuring frequency ω_I. Actually, this is a matter of the correlation time τ_c effective under the experimental conditions. $\mathscr{J}(\omega_S)$ will dominate for $\omega_S\tau_c \leq 1$ (which concomitantly means $\omega_I\tau_c \ll 1$). The time interval probed in the experiment will then be

$$\tau \approx \omega_S^{-1} \tag{1.33}$$

Likewise, if $\omega_S\tau_c \leq 1$ applies while $\omega_I\tau_c \gg 1$, the relevant time interval will be

$$\tau \approx \omega_I^{-1} \tag{1.34}$$

In the light of the above, statements concerning time scales can be made straightaway from spin–lattice relaxation dispersion curves without any model consideration. For example, a finite dispersion slope at 10 kHz indicates that correlations persist for periods longer than $\tau \geq (2\pi \times 10\ \mathrm{kHz})^{-1} \approx 1.6 \times 10^{-5}$ s in the 'like' spin case. For 'unlike' spin pairs of resonant protons and unpaired electrons and if $\mathscr{J}(\omega_S)$ dominates, the *same* dispersion features mean, however, $\tau \geq 2 \times 10^{-8}$ s. A rule of thumb is that as long as there is a finite slope of the spin–lattice relaxation dispersion, some correlation of the fluctuating interactions is retained after intervals $\tau \approx \omega_k^{-1}$,

where the subscript k indicates the leading spin transition at the current value of the external magnetic flux density.

1.1.3 The Field-cycling Principle

The main purpose of the field-cycling NMR relaxometry technique[22–25] is to measure the frequency (or field) dependence of spin relaxation parameters in as wide a range as possible. Let us first describe the measuring principle and then turn to the limits and implications of such experiments.

The thermal equilibrium of an ensemble of spins at sufficiently high temperatures is characterized by Curie's law for the magnetization:

$$\vec{M}_0 = \frac{n\gamma^2\hbar^2 I(I+1)}{3k_B T}\vec{B}_0 \tag{1.35}$$

The experimental variables are the external quantizing flux density $\vec{B}_0$ (in principle as a vector) and the absolute temperature T. The quantity n is the number density of particles bearing spins with quantum numbers I and k_B is Boltzmann's constant.

An NMR relaxation experiment begins after an abrupt perturbation of the equilibrium magnetization. That is, the initial magnetization deviates from the Curie magnetization: $\vec{M}(0) \neq \vec{M}_0$. The perturbation can be an rf pulse or – in the field-cycling case – a sharp change of $\vec{B}_0$, or both in combination.

Figure 1.4 shows a scheme of a typical *(pre-polarizing)* field cycle of the external field $B_0 = B_0(t)$. Other variants are discussed in Chapters 4, 6 and 16. After polarization of the sample by a flux density B_p, the relaxation process of interest starts in the relaxation interval with a flux density B_r. After a variable delay, the flux density is switched to the detection value B_d. An NMR signal is induced with the aid of a 90° rf pulse or a spin-echo pulse sequence. The signal amplitude will then be proportional to the magnetization retained at the end of the relaxation interval.

The flux density of the detection field is chosen as high as possible and should be as homogeneous as technically feasible for better sensitivity (see Chapter 3). Since signal acquisition takes only a few milliseconds, the detection field period can accordingly be kept short. As a consequence, the detection flux density can be particularly strong without thermally overloading the magnet coil during its duty cycle.

After signal acquisition, the flux density is switched back to the polarization field value. Allowing for an equilibrium recovery delay, the field cycle can be re-run with incremented relaxation intervals τ_r as often as needed for the point-by-point acquisition of the relaxation curve at the flux density B_r. To obtain the whole spin–lattice relaxation dispersion curve, B_r is stepped through a series of discrete values spread over the desired range. B_r is usually expressed in terms of the angular Larmor frequency $\omega = 2\pi\nu = |\gamma|B_r$ of the resonant spins.

Field cycling permits one to vary the magnetic flux density B_r while the detection field, *i.e.* the carrier frequency of the NMR spectrometer, is kept

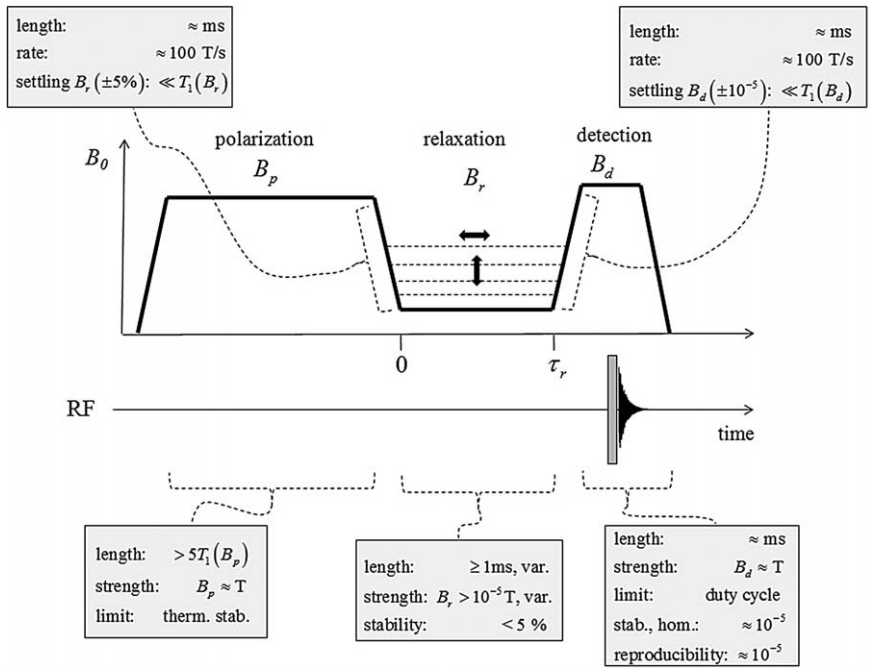

Figure 1.4 Typical specifications of the flux density variation in pre-polarized field-cycling NMR relaxometry experiments (the partial absence of quantitative numbers before the units is to be understood as 'several'). A non-equilibrium magnetization is produced by rapid switching from the polarization to the relaxation field and – after a relaxation interval – to the detection field B_d. The relaxation curve for the flux density B_r is probed point-by-point by varying the length of that interval. The signal is induced with the aid of a 90° rf pulse or a spin-echo pulse sequence. The signal amplitude is proportional to the magnetization retained at the end of the relaxation interval.
Reproduced from ref. 12 with permission. Copyright 2017 Elsevier BV.

constant. The rf unit remains permanently tuned to a fixed, predetermined frequency, *i.e.* to the resonance frequency $\nu_d = |\gamma| B_d/2\pi$, where γ is the gyromagnetic ratio of the resonant nuclei. The advantage is obvious: the rf part of the system can be optimized for the resonance frequency at the flux density B_d, while the relaxation field B_r is variable in the whole range down to lowest values feasible.

Neglecting relaxation losses during the switching down and settling time for the moment, the magnetization at the beginning of the relaxation interval is given by

$$M(0) = M_z(0) \approx M_0(B_p) \tag{1.36}$$

for the *pre-polarizing* field-cycle represented by Figure 1.4. $M_0(B_p)$ is the Curie magnetization for the flux density B_p. The magnetization then relaxes

towards the new Curie magnetization in the relaxation field, $M_0(B_r)$. Based on Bloch's equation for the z component, the magnetization decays according to

$$M_z(\tau_r) = M_0(B_r) + [M_0(B_p) - M_0(B_r)]\exp[-\tau_r/T_1(B_r)] \tag{1.37}$$

where $M_z(\tau_r)$ is the longitudinal magnetization at the end of the relaxation interval τ_r. This measurand decays from the Curie magnetization $M_0(B_p)$ in the polarization field B_p, *i.e.* $M_z(\tau_r = 0) = M_0(B_p)$, to the Curie magnetization $M_0(B_r)$ in the relaxation field B_r, that is, $M_z(\tau_r \to \infty) = M_0(B_r)$.

If the relaxation flux density B_r of interest approaches the value of the flux density B_p, the dynamic range of magnetization variation, *i.e.* $[M_0(B_p) - M_0(B_r)]$, will become too small for sensitive recording of relaxation curves. In this case, it is more favourable to use the *non-polarizing* variant of field cycling. The polarization interval is then omitted, so that the initial magnetization in the relaxation field will be $M_z(\tau_r = 0) \approx 0$ instead of $M_0(B_p)$. In this case, eqn (1.37) takes the form

$$M_z(\tau_r) = M_0(B_r)\{1 - \exp[-\tau_r/T_1(B_r)]\} \tag{1.38}$$

In eqn (1.37) and (1.38), the finite switching and settling times have not been taken into account explicitly. In the case of pre-polarization, the relaxation interval must in reality be extended from τ_r to $\tau_r + (\Delta t)_{down} + (\Delta t)_{up}$, and eqn (1.37) should be modified to

$$\begin{aligned} &M_z\left[\tau_r + (\Delta t)_{down} + (\Delta t)_{up}\right] \\ &\quad = \left\{\left(M_z\left[(\Delta t)_{down}\right] - M_0(B_r)\right)e^{-\tau_r/T_1(B_r)} + M_0(B_r)\right\}c_1 + c_2 \end{aligned} \tag{1.39}$$

where c_1 and c_2 are constants. A derivation can be found in ref. 7, p. 140. The quantity to be acquired is then

$$M_z^{detected}(\tau_r) = M_z^{\infty} + \Delta M_z^{eff} e^{-\tau_r/T_1(B_r)} \tag{1.40}$$

where M_z^{∞} and ΔM_z^{eff} are constants implicitly defined by eqn (1.39). Together with the measurand of interest, $T_1(B_r)$ or $1/T_1(B_r)$, they can be fitted to the experimental raw data. Relaxation losses in the finite switching and settling intervals obviously diminish the dynamic range of the variation of the relaxation decay and, hence, the experimental accuracy. However, they do not cause any systematic experimental error provided that the passages between the different field levels are reproducible when incrementing the relaxation interval τ_r for a given relaxation flux density B_r. The limitation of field-cycling NMR relaxometry with respect to the finite switching intervals is thus given by the requirement that ΔM_z^{eff}, *i.e.* the dynamic range of signal variations, should be large enough for good signal acquisition sensitivity.

In representations of field-cycling NMR relaxometry data, it is most important that specifications characterizing the evaluated relaxation curves are included. This in particular refers to whether and how far the curves can indeed be represented by monoexponential decays anticipated in eqn (1.37)–(1.40). Reasons for deviations will be discussed in Section 1.2.1. If monoexponential fits are employed, the resulting relaxation data should be supplemented by specifying the range (in terms of orders of magnitude) over which the curves can be described by monoexponential functions, and with what standard deviation. Diagrams of data processed further than needed for the primary evaluation of relaxation curves may conceal the direct information derived from the measuring process and should therefore be used at the acquisition stage only if unavoidable.

1.1.4 Technical Limits

Typical field-cycling magnet coils are made of diamagnetic materials. They are mounted in setups that do not contain any conducting loops that might give rise to eddy currents upon switching the field. The magnetic energy will essentially be deposited in the space in and around the magnet. All technical challenges that the design of field-cycling NMR relaxometers may demand thus originate from the need to transport large amounts of magnetic field energy

$$W_{\mathrm{magn}} = \frac{1}{2\mu_0}\int_{\mathrm{volume}} B_0^2(\vec{r})\mathrm{d}^3 r \tag{1.41}$$

from and to the magnetic-field filled space in a precise, fast and well-controlled way. W_{magn} will be large for voluminous magnets and small for compact architectures. Large magnets favour good detection field homogeneities, large sample volume and efficient cooling devices. In the present context, good field homogeneity is mainly desirable for the sensitivity of signal detection. Signals of liquid-like samples can then be acquired with an accordingly narrow rf bandwidth serving the suppression of noise. On the other hand, compact magnets facilitate fast field switching. Desirable specifications are listed in the insets in Figure 1.4. Technical compromises developed for the optimization of such characteristics are described and discussed in detail in Chapters 3–5.

Good sensitivity requires polarization and detection flux densities, B_{p} and B_{d}, respectively, that are as high as possible with reasonable homogeneity and sufficient thermal stability. Field switching and settling times limit the range of relaxation times that can be measured. At the lowest fields, spin–lattice relaxation times can be less than 1 ms even in diamagnetic samples, depending on molecular dynamics and spin couplings. The field switching intervals must be correspondingly short. The problem is not so much to ensure high field slew rates. Rates of about 10^3 T s^{-1} are easy to reach in principle. The difficulty is rather to *settle and stabilize* the field with the

desired precision after the relaxation flux density has been reached. For the relaxation interval, an accuracy of a few percent in a settling time of less than 1 ms after lowering the field is normally considered to be sufficient. A discussion of how this specification can technically be validated and calibrated is presented in Chapters 3 and 4.

Field-cycling NMR relaxometry requires instruments dedicated to this particular version of NMR experiments. To some limited extent, information on the low-frequency dispersion of spin–lattice relaxation can also be examined with the aid of rotating-frame techniques (see Chapter 7), which can be implemented on conventional high-field spectrometers. The accessible frequency range of ordinary on-resonance rotating-frame NMR relaxometry[26] can be extended by an off-resonance variant.[27] Moreover, a rotating-frame analogue of field-cycling relaxometry exists, termed SLOAFI (spin-lock adiabatic field-cycling imaging). It enables one to probe low-frequency rotating-frame spin–lattice relaxation in a certain frequency range without stepping the rotating rf flux density.[28,29] As already mentioned, the application of rotating-frame techniques is of particular interest for samples with strongly restricted reorientation processes such as liquid crystals,[17] where the relation given in eqn (1.18) is suspected to fail.

1.1.5 Physical Limits

As demonstrated in Chapters 3–5, the *technical* difficulties concerning the lowest frequencies that can be reached, and the short field switching and settling times that are needed, appear to be largely overcome with the present state of the art. Hence the question remains of whether *physical* limits exist that restrict applications in these respects.

1.1.5.1 Intrinsic Low-frequency Limits

In principle, there are two physical, *i.e.* sample-dependent, reasons why measurements and interpretations at extremely low frequencies might become doubtful. The first reason, the *violation of the Redfield condition* requiring $T_1 \gg \omega_k^{-1}$ has already been referred to in the context of eqn (1.15), (1.21) and (1.27), where ω_k is the angular spin transition frequency for which the spectral density $\mathcal{J}(\omega_k)$ provides the leading contribution under the experimental conditions. This situation may arise if strong spin interactions, *i.e.* short spin–spin distances and/or efficient electron paramagnetic coupling partners. The consequence will be a low-frequency cut-off of the relaxation dispersion. Importantly, this must not be confused with the proper low-frequency plateau expected for $\omega\tau_c \ll 1$ (compare the exemplary spectral densities plotted in Figure 1.3). Therefore, some care is appropriate at proton frequencies of a few kilohertz if spin–lattice relaxation times turn out to be below a few milliseconds. The same limitation will be effective for spin–lattice relaxation in the rotating frame.

In certain systems, fast restricted fluctuation components, *e.g.* rotational diffusion about a preferential axis, are superimposed to slow isotropic reorientation processes. While the former tends to comply with the Redfield condition in the whole field-cycling frequency range, the latter may violate it. This can give rise to a further origin of low-frequency artefacts. It has to do with so-called *local fields produced by secular spin interactions*.

The attribute 'secular' means that no or at most spin energy-conserving transitions (*i.e.* zero-quantum transitions as illustrated in Figure 1.1a) are induced by the respective terms of the Hamiltonians given in eqn (1.8) and (1.19). For homonuclear spin pairs labelled with subscripts k and l, the *secular* part of the dipolar Hamiltonian eqn (1.8) is[2,7]

$$\mathscr{H}_{kl}^{(\mathrm{d,sec})} = \frac{\mu_0}{4\pi}\frac{\gamma^2\hbar^2}{r_{kl}^3}\frac{1}{2}\left(1 - 3\cos^2\vartheta_{kl}\right)\left[3I_{kz}I_{lz} - \left(\vec{I}_k \cdot \vec{I}_l\right)\right] \tag{1.42}$$

where I_{kz} and I_{lz} represent the z components of the spin vector operators $\vec{I}_k$ and $\vec{I}_l$, respectively.

For rotationally symmetric electric field gradients, the secular part of the quadrupolar high-field Hamiltonian eqn (1.19) is likewise represented by[2,7]

$$\mathscr{H}^{(\mathrm{q,sec})} = \frac{e^2qQ}{4I(2I-1)}\frac{3}{2}\left(3\cos^2\vartheta - 1\right)\left[3I_z^2 - \vec{I}^2\right] \tag{1.43}$$

where I_z is the z component of the spin vector operator $\vec{I}$.

For *unrestricted* and – relative to the spin–lattice relaxation rate – *fast* molecular motions, the secular Hamiltonians are effectively averaged to zero:

$$\left\langle \mathscr{H}^{(\mathrm{d,sec})} \right\rangle_{\tau \approx T_1} \to 0, \quad \left\langle \mathscr{H}^{(\mathrm{q,sec})} \right\rangle_{\tau \approx T_1} \to 0 \tag{1.44}$$

The angular brackets indicate temporal averages on the time scale $\tau \approx T_1$, *i.e.* relative to the mean lifetime of spin states. This is in contrast to cases where molecular dynamics is strongly constrained, such as in liquid crystals or polymer systems. *Motional averaging* can then no longer be taken for granted, and residual *local fields* may arise.

The *unaveraged dipolar magnetic fields* $\delta\vec{B}_{\mathrm{dip}} = \delta\vec{\omega}_{\mathrm{dip}}/\gamma$ from dipolar couplings can be represented by the mean angular precession frequency $\omega_{\mathrm{loc}} = \sqrt{\left\langle \delta\omega_{\mathrm{dip}}^2 \right\rangle_{\tau \approx T_1}}$. Likewise, *unaveraged electric field gradients* suggest $\omega_{\mathrm{loc}} = \sqrt{\left\langle \delta\omega_{\mathrm{q}}^2 \right\rangle_{\tau \approx T_1}}$. The angular frequencies ω_{loc} would be relevant for spin precession if solely these residual fields were to exist. The respective values can reach 10^5 rad s^{-1} for protons and 10^6 rad s^{-1} for deuterons in extreme cases. These local fields may exceed the external field B_0 at low frequencies and, hence, govern quantization. Field-cycling NMR relaxometry must therefore

comply with the *high-field condition* $B_0 \gg B_{loc}$, where $B_{loc} = \omega_{loc}/|\gamma|$. Needless to say, spin–lattice relaxation in the rotating frame is restricted by analogous conditions, *i.e.* $T_{1\rho} \gg \omega_1^{-1}$ and $\omega_1 \gg \omega_{loc}$ (see Chapter 7). Further features of systems with motional restrictions are discussed in Section 1.3.3.

The difference in low-frequency artefacts due to violation of the Redfield condition on the one hand and to local fields on the other applies only to systems with *motional restrictions* on time scales longer than T_1. In the case of *isotropic* fluctuations, motional averaging of local fields on the time scale of T_1 is already warranted in the Redfield limit. Both sources of potential low-frequency artefacts will then be excluded concomitantly if $T_1 \gg \omega_k^{-1}$ is satisfied.

1.1.5.2 Intrinsic Fast Field-switching Limit

With respect to the dynamic signal detection range and concerning the measurability of extremely short relaxation times, one may conclude that 'fast is always better than slow'. However, if the slew rate is too high and if the angular Larmor frequency vector $\vec{\omega}_{ext} = -\gamma\vec{B}_0$ in the external field $\vec{B}_0$ reaches magnitudes smaller than the arbitrarily oriented Larmor frequency $\vec{\omega}_{loc}$ in the local fields, so-called *zero-field coherences*[23,30] can be excited. This is a spectroscopic phenomenon totally different from relaxation processes. In order to avoid such effects, an *adiabatic* crossover between the polarization and relaxation intervals should be approached. The field variation rate must be slow relative to the instantaneous Larmor precession. The condition for adiabatic field transitions is[31,32]

$$\frac{1}{\omega^2}\left|\vec{\omega} \times \frac{\partial\vec{\omega}}{\partial t}\right| \ll \omega \tag{1.45}$$

where $\vec{\omega} = \vec{\omega}_{ext} + \vec{\omega}_{loc}$.

1.2 Exchange in Heterogeneous and Multi-phase Systems

Time scales are a key issue in field-cycling NMR relaxometry. This applies in particular to heterogeneous and multi-phase systems where exchange processes matter. Spin–lattice relaxation depends on material properties such as *molecular mobilities*, *steric restrictions*, *strength of spin interactions*, *microstructural constraints*, *electron paramagnetic centres*, *etc.* If these features are distributed inhomogeneously in the sample, the crucial question arises of whether levelling by exchange is effective or not. The problem to be dealt with is illustrated in Figure 1.5.

The relevant exchange mechanisms are normally of a physicochemical nature. However, exchange between dipolar-coupled protons can also be mediated by *immaterial spin transport*. With solids or solid-like materials,

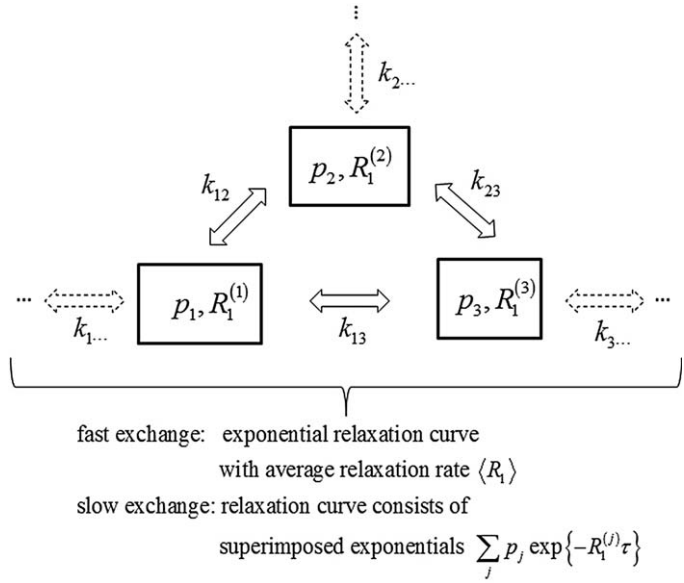

Figure 1.5 Schematic network of compartments or phases in a heterogeneous sample with different local spin–lattice relaxation rates. Depending on the molecular or spin exchange rates k_{ij} between 'sites' i, j, the spin–lattice relaxation curves will be monoexponential for fast exchange and multiexponential for slow exchange.

one speaks of *spin diffusion*, whereas immaterial spin transport in liquids is better referred to as *cross-relaxation*.[5]

In dipolar-coupled, homonuclear spin systems, pair-wise exchange between spins labelled with subscripts k and l is induced by the flip-flop Hamilton operator[‡‡]:

$$\mathscr{H}_{kl}^{(\mathrm{d,ff})} = -\frac{\mu_0}{4\pi}\gamma^2\hbar^2\frac{1}{4}\frac{(1-3\cos^2\vartheta_{kl})}{r_{kl}^3}(I_k^+I_l^- + I_l^-I_k^+) \qquad (1.46)$$

It produces zero-quantum transitions (compare Figure 1.1a) corresponding to an exchange of spin states between the two nuclei involved. Effectively, this means *diffusive transport* of spin states from spin-bearing nucleus to spin-bearing nucleus. I_k^-, I_l^- and I_l^+, I_k^+ are the respective lowering and raising spin operators.[7]

Spin diffusion will not be effective for quadrupole nuclei such as deuterons, for which homonuclear dipolar coupling is relatively weak. Note, furthermore, that exchange between spatially extended phases will be controlled by translational diffusion and – if existing – by spin diffusion from

[‡‡]Eqn (1.46) is the flip-flop part of the secular Hamiltonian given in eqn (1.42). Note that homonuclear flip-flop spin transitions are an intrinsic part of *transverse* relaxation,[2,3,5,7] so that they do not contribute to exchange averaging in this case.

and to the interfaces between the phases. It can therefore be much slower than expected for direct thermal activation. In the following, we will distinguish the time scale of the *relaxation process* from that of the *autocorrelation function*.

1.2.1 Exponential and Non-exponential Relaxation Curves

It is often taken for granted that relaxation curves are *monoexponential*. Fortunately, this is normally – but definitely not always – the case, even in heterogeneous or multi-phase samples. The criterion is the exchange rates between the phases relative to relaxation rates.

1.2.1.1 Fast Exchange on the Relaxation Time Scale

If molecular or spin exchange rates between sites of different relaxation efficiency are much greater than the local spin–lattice relaxation rates, *i.e.* $k_{ij} \gg R_1^{(i)}, R_1^{(j)}$, the relaxation curves will be monoexponential:

$$\frac{M_z(\tau) - M_0(B_r)}{M_0(B_p) - M_0(B_r)} = \exp(-\langle R_1 \rangle \tau) \tag{1.47}$$

They decay with the average spin–lattice relaxation rate $\langle R_1 \rangle = \sum_j \left[p_j \Big/ T_1^{(j)} \right]$. The local rates $R_1^j = 1/T_1^{(j)}$ that would be effective at the 'sites' j in the absence of exchange are weighted by the respective populations p_j (see Figure 1.5).

1.2.1.2 Slow Exchange on the Relaxation Time Scale

In the opposite limit, $k_{ij} \ll R_1^{(i)}, R_1^{(j)}$, exchange will be too slow to level the local relaxation rates. The relaxation curves will then be composed of a distribution of exponentials:

$$\frac{M_z(\tau) - M_0(B_r)}{M_0(B_p) - M_0(B_r)} = \sum_j p_j \exp\left[-R_1^{(j)} \tau \right] \tag{1.48}$$

Slow exchange is relevant in composite media, where grains of different molecular mobility and/or spin couplings are larger than the root mean-square spin displacements on the time scale of spin–lattice relaxation, be it by chemical or by flip-flop exchange.

In principle, non-exponential relaxation curves of the type eqn (1.48) can be analysed in terms of superimposed exponential components using the inverse Laplace transform (ILT) evaluation procedure (see, *e.g.*, Chapters 10, 18 and 19). Another approach that is independent of the dynamic signal range recorded or reached in the experiments is to evaluate directly the *average* relaxation rate from non-exponential relaxation curve data.

The normalized distribution of (local) relaxation rates in the absence of exchange be $g(R_1)$. The spin–lattice relaxation curve is then expressed as

$$\frac{M_z(\tau) - M_0(B_r)}{M_0(B_p) - M_0(B_r)} = \int_0^\infty g(R_1) \exp(-R_1\tau) \mathrm{d}R_1 \tag{1.49}$$

Actually, this is the integral version of eqn (1.48). The slope of the relaxation curve is given by

$$\frac{\partial}{\partial\tau}\left[\frac{M_z(\tau) - M_0(B_r)}{M_0(B_p) - M_0(B_r)}\right] = -\int_0^\infty g(R_1) R_1 \exp(-R_1\tau) \mathrm{d}R_1 \tag{1.50}$$

The initial slope

$$\lim_{\tau\to 0}\frac{\partial}{\partial\tau}\left[\frac{M_z(\tau) - M_0(B_r)}{M_0(B_p) - M_0(B_r)}\right] = -\int_0^\infty g(R_1) R_1 \mathrm{d}R_1 = -\langle R_1\rangle \tag{1.51}$$

obviously renders the *exact* average of the local relaxation rates. To obtain this information, there is no need to acquire the whole relaxation curve. The average in eqn (1.51) is moreover *identical* with the average obtained in the fast spin-exchange limit eqn (1.47): the result for fictitious levelling by fast exchange in the sample is the same as post-experimental averaging in the absence of exchange *via* the initial slope.

In practice, one can determine the initial slope of the relaxation curve by taking the numerical derivative of the experimental data set and extrapolating to the origin of the relaxation interval. Alternatively, even a simple fit of an exponential function to the first few data points should be sufficient for a reasonable approach. In cases where neither the slow- nor the fast-exchange limit applies, the situation may be less clear. However, the above evaluation protocol for the slow-exchange limit will nevertheless provide characteristic and reproducible values.

1.2.2 Exchange Relative to the Time Scale of Correlation Functions

The fast exchange limit on the *relaxation time scale*, *i.e.* relative to local relaxation times, can be further subdivided into fast- and slow-exchange limits relative to the time scale on which *correlation functions* are probed. For discussion purposes, we will restrict ourselves to a system consisting of two phases in which molecules are subject of different correlation decays. As an illustrative – but certainly not exclusive – example, we will consider polar fluids in porous or colloidal media with polar surfaces where one can distinguish an adsorbed fluid phase and a bulk-like fluid phase (see Figure 1.6).

Furthermore, we will restrict ourselves to *intramolecular* orientation correlation functions:

$$\mathcal{G}(\tau) \approx \mathcal{G}_k(\tau) = 4\pi(-1)^k \langle Y_{2,k}(0)\, Y_{2-k}(\tau)\rangle \tag{1.52}$$

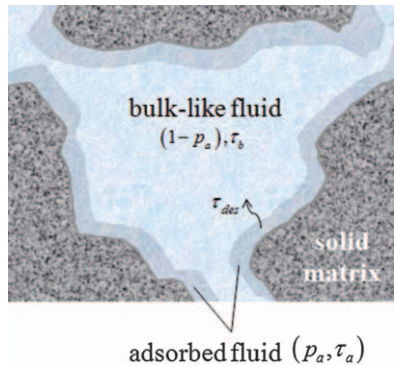

Figure 1.6 Schematic representation of the two-phase-exchange model of fluids confined in saturated porous matrices. The fluid adsorbed at surfaces (population p_a and correlation time τ_a) is distinguished from the bulk-like phase (population $1-p_a$ and correlation time τ_b). Molecular mobilities within and exchange kinetics between these phases determine the dynamics of fluid molecules. The mean desorption time in the adsorbed phase is denoted τ_{des}. The limits $T_1(\omega) \gg \tau \gg \tau_{\mathrm{des}}$ (fast exchange on both the relaxation and correlation time scales) and $T_1(\omega) \gg \tau_{\mathrm{des}} \gg \tau$ (fast exchange on the relaxation time scale, slow exchange on the correlation time scale) are of particular interest.

Four different scenarios can be distinguished. They are characterized by the following mutually exclusive probabilities: (a) $f_{a,a}(\tau)$, fraction of molecules that happen to be initially (= time 0) and also finally (= time τ) in the adsorbed phase; (b) $f_{a,b}(\tau)$, fraction of molecules that happen to be initially in the adsorbed phase and finally in the bulk-like phase; (c) $f_{b,a}(\tau)$, fraction of molecules that happen to be initially in the bulk-like phase and finally in the adsorbed phase; and (d) $f_{b,b}(\tau)$, fraction of molecules that happen to be initially and also finally in the bulk-like phase. Normalization requires

$$f_{a,a}(\tau) + f_{a,b}(\tau) + f_{b,a}(\tau) + f_{b,b}(\tau) = 1 \tag{1.53}$$

The subscripts a and b stand for 'adsorbed' and 'bulk-like', respectively. Cases (a) and (d) imply that a reference molecule will be still or again in the same phase as initially. This is in contrast to cases (b) and (c), where the initial and final phases are different.

From the statistical point of view, eqn (1.52) can be subdivided into four partial correlation functions for four sub-ensembles of molecules. The total correlation function effective for all molecules in both phases is then the weighted average[§§]:

$$\mathcal{G}(\tau) = f_{a,a}(\tau)\,\mathcal{G}_{a,a}(\tau) + f_{a,b}(\tau)\,\mathcal{G}_{a,b}(\tau) + f_{b,a}(\tau)\,\mathcal{G}_{b,a}(\tau) + f_{b,b}(\tau)\,\mathcal{G}_{b,b}(\tau) \tag{1.54}$$

[§§]Remember that we are dealing with the fast-exchange limit on the relaxation time scale.

The partial correlation functions $\mathcal{G}_{i,j}(\tau)$ for $i = a,b$ and $j = a,b$ refer to sub-ensembles of molecules being initially in phase *i and* finally in phase *j*. Their contributions are weighted by the fractions $f_{i,j}$.

The local correlation times in the adsorbed and bulk-like phases, that is, the time constants of $\mathcal{G}_{a,a}(\tau)$ and $\mathcal{G}_{b,b}(\tau)$, are denoted τ_a and τ_b, respectively. The correlation time in the bulk medium can be assumed to be short relative to that of the adsorbed phase: $\tau_b \ll \tau_a$. Restricting ourselves to intervals $\tau > \tau_b$ means that all correlation will have faded away if molecules reside in the bulk phase permanently or temporarily: $\mathcal{G}_{a,b}(\tau > \tau_b) \approx 0$, $\mathcal{G}_{b,a}(\tau > \tau_b) \approx 0$ and $\mathcal{G}_{b,b}(\tau > \tau_b) \approx 0$. Eqn (1.54) is thus reduced to

$$\mathcal{G}(\tau > \tau_b) \approx f_{a,a}(\tau)\mathcal{G}_{a,a}(\tau) \tag{1.55}$$

so that τ_a remains as the correlation time of particular interest here[¶¶].

With the mean desorption time τ_{des} of molecules in the adsorbed phase, fast- and slow-exchange limits can be defined relative to the interval τ after which the correlation function $\mathcal{G}_{a,a}(\tau)$ is considered:

$$\left.\begin{array}{l} \tau \gg \tau_{\mathrm{des}} \rightarrow \text{fast} \\ \tau \ll \tau_{\mathrm{des}} \rightarrow \text{slow} \end{array}\right\} \text{desorption on the time scale } \tau > \tau_b \tag{1.56}$$

1.2.2.1 Fast Exchange Relative to the Correlation Time Scale

In the *fast-exchange limit* relative to the correlation time scale $\tau \gg \tau_{\mathrm{des}}$, the probabilities of finding the reference molecule in the adsorbed phase initially and finally are *independent* of each other. The fraction $f_{a,a}$ can therefore be approximated by

$$f_{a,a}(\tau \gg \tau_{\mathrm{des}}) \approx p_a^2 \tag{1.57}$$

where p_a is the (time independent) population in the adsorbed phase. Eqn (1.55) can thus be expressed by

$$\mathcal{G}(\tau) \approx p_{\mathrm{a}}^2 \mathcal{G}_{a,a}(\tau) \quad \text{for} \quad \tau_b < \tau \gg \tau_{\mathrm{des}} \tag{1.58}$$

1.2.2.2 Slow Exchange Relative to the Correlation Time Scale

In the opposite limit of *slow exchange* relative to the correlation time scale, $\tau \ll \tau_{\mathrm{des}}$, the adsorbate molecules will remain in their initial phase, so that

$$f_{a,a}(\tau \ll \tau_{\mathrm{des}}) \approx p_a \tag{1.59}$$

The correlation function eqn (1.55) thus adopts the form

$$\mathcal{G}(\tau\rangle \approx p_{\mathrm{a}} \mathcal{G}_{a,a}(\tau) \quad \text{for} \quad \tau_b < \tau \ll \tau_{\mathrm{des}} \tag{1.60}$$

The remarkable difference between eqn (1.58) and (1.60) is that the former has a *quadratic* and the latter a *linear* dependence on the population of the

[¶¶]The term 'correlation time' is understood as defined in eqn (1.5).

adsorbed phase. On the other hand, the decay of the effective correlation function of all particles in both phases will be dominated by the sub-ensemble residing both initially and finally in the adsorbed phase. That is, the function $\mathcal{G}_{a,a}(\tau)$ matters in either case.

1.2.2.3 Dependences on Populations

The spectral densities conjugate to eqn (1.58) and (1.60) are

$$\mathcal{J}_{aa}(\omega) = p_a^2 \int_{-\infty}^{+\infty} \mathcal{G}_{a,a}(\tau)\, \mathrm{e}^{-i\omega\tau} \mathrm{d}\tau \quad \text{for} \quad \frac{1}{\tau_b} > \omega \ll \frac{1}{\tau_{\mathrm{des}}} \tag{1.61}$$

for fast exchange and

$$\mathcal{J}_{aa}(\omega) = p_a \int_{-\infty}^{+\infty} \mathcal{G}_{a,a}(\tau)\, \mathrm{e}^{-i\omega\tau} \mathrm{d}\tau \quad \text{for} \quad \frac{1}{\tau_{\mathrm{des}}} \ll \omega < \frac{1}{\tau_b} \tag{1.62}$$

for slow exchange. According to these limits, a distinction is possible *via* the proportionalities

$$\frac{1}{T_1(\omega)} \propto p_a^2 \quad \text{for} \quad \frac{1}{\tau_b} > \omega \ll \frac{1}{\tau_{\mathrm{des}}} \tag{1.63}$$

predicted for *fast exchange on both the correlation and relaxation time scales*, and

$$\frac{1}{T_1(\omega)} \propto p_a \quad \text{for} \quad \frac{1}{\tau_{\mathrm{des}}} \ll \omega < \frac{1}{\tau_b} \tag{1.64}$$

for *slow desorption on the correlation time scale but fast exchange on the relaxation time scale*. In this respect, experiments and Monte Carlo simulations have been reported.[17,33] Note that the relevant angular frequency in eqn (1.63) and (1.64) is $\omega \approx |\gamma| B_0$ in the 'like' spin case, whereas it can be either $\omega_I \approx |\gamma_I| B_0$ or $\omega_S \approx |\gamma_S| B_0$ for 'unlike' spin systems depending on the spectral density dominating under the experimental conditions (see Section 1.1.2).

1.2.2.4 Solutions of Paramagnetic Ions or Molecules

The solvation shell of paramagnetic particles can be identified with the 'adsorbed phase'. Examples are aqueous solutions of paramagnetic ions or paramagnetic globular proteins. According to eqn (1.81), which is derived in Section 1.3.2, the effective correlation time for dipolar couplings in the solvation shells is[34–36]

$$\frac{1}{\tau_a} = \frac{1}{\tau_{\mathrm{rot}}} + \frac{1}{\tau_S} + \frac{1}{\tau_{\mathrm{des}}} \tag{1.65}$$

where τ_{rot} is the correlation time for rotational diffusion of the salvation complex and τ_S is the flip time of the unpaired electron spin. Diamagnetic

relaxation mechanisms in both the bulk and adsorbed phases are assumed to be negligible. Since normally $\tau_{rot} \ll \tau_S, \tau_{des}$, the correlation time scale of interest will be $\tau_b < \tau \approx \tau_{rot} \ll \tau_{des}$. That is, the slow-exchange limit will be relevant for $1/\tau_b > \omega > 1/\tau_{des}$, and the *linear* relationship eqn (1.64) applies.

1.2.2.5 Paramagnetic Ions Fixed at Solid Pore Surfaces

If paramagnetic particles are fixed at pore surfaces (see Chapters 18–20) or if scalar interaction[2,7] dominates, rotational diffusion cannot contribute to fluctuations of the interactions between the dipoles in the solvent and those of the unpaired electrons. Eqn (1.65) is thus reduced to

$$\frac{1}{\tau_a} = \frac{1}{\tau_S} + \frac{1}{\tau_{des}} \tag{1.66}$$

If $\tau_S \ll \tau_{des}$, the correlation time scale of interest will be $\tau_b < \tau \approx \tau_S \ll \tau_{des}$, so that the slow exchange limit will apply for $1/\tau_b > \omega > 1/\tau_{des}$, as before. Conversely, in the limit $\tau_S \gg \tau_{des}$, slow or fast exchange will be relevant depending on whether the correlation time scale is $\tau_b < \tau < \tau_{des}$ or $\tau_b < \tau > \tau_{des}$. With increasing time interval τ or decreasing angular frequency ω, there will be a crossover from the slow to the fast exchange limit, *i.e.* from the linear relationship eqn (1.64) to the quadratic counterpart eqn (1.63).

1.2.2.6 The RMTD Case

The RMTD process[13,37] of adsorbate molecules at surfaces refers to entirely diamagnetic materials. In addition to the discussion in Section 1.1.1.3 on the special intra- and intermolecular relaxation features of this mechanism, there is one more peculiar characteristic, namely the exchange behaviour. Desorption does not mean final loss of all rotational and translational correlations of spin interactions. After readsorption and subject to the surface topology, molecules can *regain* an orientation correlated to the orientation before desorption (for an illustration, see Figure 1.7c).

As a consequence, the time scale τ on which the correlation function $\mathcal{G}_{a,a}(\tau)$ is still finite is much longer than the desorption time τ_{des} characterizing the intermittent periods that adsorbate molecules spend on the surface between adsorption and desorption. τ_{des} can in principle be measured in a separate experiment with samples having electron paramagnetic centres incorporated in the surface (see the previous section). If these centres dominate spin–lattice relaxation, all diamagnetic processes including RMTD can be neglected. Values for the desorption time found under such conditions are of an order of magnitude similar to that of solutions of paramagnetic ions,[34–36] *i.e.* $\tau_{des} \approx 10^{-8}$–$10^{-7}$ s (see Chapters 18–20)[‖‖]. This can be compared with correlation times τ_a found in diamagnetic samples of

[‖‖]Here we tacitly identify hydration shells of ions in solution with the adsorption phase of porous media.

the same porosity, which are several orders of magnitude longer.[13,37] The RMTD process of adsorbate molecules must therefore consist of numerous desorption/bulk excursion/readsorption intermezzos before the autocorrelation function finally fades away subject to the surface topology. From the statistical point of view, this mechanism implies features of Lévy walks, as can nicely be demonstrated by computer simulations.[38]

An order of magnitude $\tau_{\mathrm{des}} \approx 10^{-8}$ s means that for $\omega < \tau_{\mathrm{des}}^{-1} \approx 10^{8}$ rad s^{-1} we have fast exchange and for $\omega > \tau_{\mathrm{des}}^{-1} \approx 10^{8}$ rad s^{-1} slow exchange on the time scale τ to be probed in experiments. There will again be a crossover from a quadratic dependence on the population in the adsorbed phase at low frequencies to a linear relationship at higher values.

1.3 Remarks on Correlation Functions and Their Parallelism with Relaxation Functions

1.3.1 Calculation of Correlation Functions

Let us consider an (unnormalized) autocorrelation function of the type defined in eqn (1.11) and (1.22):

$$G(\tau) = C\langle F(0)F^{*}(\tau)\rangle \tag{1.67}$$

where C is a constant, and where we have omitted all sub- and superscripts used in the formalisms above. The angular brackets in eqn (1.67) stand for ensemble averages, and the time scale is limited by $\tau < T_1$. All molecular motions and – *nota bene* – exchange processes taking place within this period are relevant and must therefore be considered. Generally, the evaluation of ensemble averages for the dynamic model under consideration is a matter of probability treatments.

For definitions, the reader is referred to the dipolar-coupling scenario illustrated in Figure 1.2. The *conditional* probability density for the initial and final values of the functions $F_i \equiv F[\varphi(0), \vartheta(0), r(0)]$ and $F_f \equiv F[\varphi(\tau), \vartheta(\tau), r(\tau)]$, respectively, is termed $P_c(F_i, F_f; \tau)$. In other words, $P_c(F_i, F_f; \tau)$ is the probability density that the value after the interval τ will be F_f if the initial value was F_i. We speak of a probability *density* since it concerns a volume element $\mathrm{d}V_f$ around the spherical coordinate triple $\varphi(\tau), \vartheta(\tau), r(\tau)$.

Furthermore, let $p(F_i)$ be the *a priori* probability density for the initial value F_i with regard to a volume element $\mathrm{d}V_i$ around the starting coordinates $\varphi(0)$, $\vartheta(0), r(0)$. The expression $p(F_i)P_c(F_i, F_f; \tau)\mathrm{d}V_i\mathrm{d}V_f$ is then the (unconditional) probability that the function F has the initial value F_i and the value F_f finally.

With these definitions, the ensemble average of the autocorrelation function $G(\tau)$ in eqn (1.67) is calculated by integrating over the sample volume according to

$$G(\tau) = \int\int F_i F_f^{*} P(F_i, 0; F_f, \tau)\mathrm{d}V_i\mathrm{d}V_f = \int\int F_i F_f^{*} p(F_i) P_c(F_i, F_f; \tau)\mathrm{d}V_i\mathrm{d}V_f \tag{1.68}$$

Given a certain concept for molecular dynamics, the task to be performed is the evaluation of the corresponding probability densities specific for that model.

An instructive – but definitely not ubiquitous – case is the intramolecular relaxation mechanism due to *isotropic rotational diffusion* (see the illustration in Figure 1.7a).[2,5] The orientation of an inter-dipole vector at time t is defined by the unit vector $\vec{u}(t)=\vec{r}(t)/r$ with the polar coordinates $\varphi(t)$, $\vartheta(t)$, $u=1$ length unit. Let us now consider the time interval between $t=0$ and $t=\tau$. With the identities $\varphi(0)\equiv\varphi_i$, $\vartheta(0)\equiv\vartheta_i$, $\vec{u}(0)\equiv\vec{u}_i$ and $\varphi(\tau)\equiv\varphi_f$, $\vartheta(\tau)\equiv\vartheta_f$, $\vec{u}(\tau)\equiv\vec{u}_f$ for the respective initial and final orientations, the normalized autocorrelation function for dipolar coupling at fixed inter-dipole distance reads

$$\mathcal{G}_k(\tau)=4\pi(-1)^k\left\langle Y_{2,k}(\vec{u}_i)Y_{2,-k}\left(\vec{u}_f\right)\right\rangle \tag{1.69}$$

[see eqn (1.12)].

The ensemble average over all possible initial and final orientations can be calculated as suggested by the probability expression eqn (1.68). In this context, the term *probability density* refers to solid angles instead of volumes in the proper sense. The probability that the final unit vector $\vec{u}_f$ points in a solid-angle element $\mathrm{d}\Omega_f=\sin\vartheta_f\mathrm{d}\vartheta_f\mathrm{d}\varphi_f$ *and* that the initial unit vector $\vec{u}_i$ points in the solid-angle element $\mathrm{d}\Omega_i=\sin\vartheta_i\mathrm{d}\vartheta_i\mathrm{d}\varphi_i$ is thus equal to $P(\vec{u}_i,0;\vec{u}_f,\tau)\ \sin\ \vartheta_f\ \sin\vartheta_i\mathrm{d}\vartheta_f\mathrm{d}\varphi_f\mathrm{d}\vartheta_i\mathrm{d}\varphi_i$, where $P(\vec{u}_i,0;\vec{u}_f,\tau)$ is the corresponding

Figure 1.7 Exemplary model scenarios for molecular reorientation processes with and without restrictions. (a) Unrestricted isotropic rotational diffusion of more or less spherical molecules bearing two dipoles $\vec{\mu}_I$ and $\vec{\mu}_S$. The cones symbolize precession about the external flux density $\vec{B}_0$. A typical example is rotational diffusion of the hydration complexes of electron-paramagnetic ions in aqueous solutions (see, *e.g.*, ref. 35 and 36). (b) Fast but restricted polymer segment reorientations by fluctuating rotational isomerism superimposed by slow Rouse chain modes (see Chapters 8 and 13 and ref. 18). (c) RMTD process: adsorbate molecules diffuse along a more or less rough surface of a solid adsorbent (see ref. 13 and 37). While being adsorbed at the surface, molecules are subject to fast and restricted rotational diffusion. This can be superimposed by a (slow) displacement process along the surface *via* excursions to the bulk fluid. After readsorption, the initial orientation $\vec{u}_\mathrm{i}$ will be converted to the final orientation $\vec{u}_\mathrm{f}$ controlled by the local surface topology. In a sequence of numerous 'desorption/(diffusive bulk excursion)/readsorption' cycles, adsorbate molecules can intermittently probe surfaces in this way over relatively long distances while – as per surface topology – they retain orientation correlations orders of magnitude longer than the actual surface residence times during the sporadic adsorption events. Reproduced from ref. 12 with permission. Copyright 2017 Elsevier BV. (d) Order-director fluctuations collectively reorient molecules on a time scale much longer than restricted rotational diffusion about the long-axis of the molecules (see Chapter 11 and ref. 5).

probability density. Likewise, the *a priori* probability that the unit vector $\vec{u}_i$ points in a solid-angle element $\mathrm{d}\Omega_i = \sin\vartheta_i \mathrm{d}\vartheta_i \mathrm{d}\varphi_i$ equals $p(\vec{u}_i)\ \sin\vartheta_i \mathrm{d}\vartheta_i \mathrm{d}\varphi_i$, where $p(\vec{u}_i)$ is the *a priori* probability density. Eventually, the conditional probability that the final unit vector $\vec{u}_f$ points in the solid-angle element $\mathrm{d}\Omega_f = \sin\vartheta_f \mathrm{d}\vartheta_f \mathrm{d}\varphi_f$ if the initial unit vector is $\vec{u}_i$ is defined by $P_c(\vec{u}_i, \vec{u}_f, \tau)\sin\vartheta_f \mathrm{d}\vartheta_f \mathrm{d}\varphi_f$, where $P_c(\vec{u}_i, \vec{u}_f, \tau)$ is the conditional probability density. In summary, we thus obtain

$$\begin{aligned} \mathcal{G}_k(\tau) = 4\pi(-1)^k \int_0^{2\pi} \mathrm{d}\varphi_f \int_0^{\pi} \mathrm{d}\vartheta_f \int_0^{2\pi} \mathrm{d}\varphi_i \int_0^{\pi} \mathrm{d}\vartheta_i p(\vec{u}_i) \\ \times P_c\left(\vec{u}_i, \vec{u}_f, \tau\right) Y_{2,k}(\vec{u}_i) Y_{2,-k}\left(\vec{u}_f\right) \sin\vartheta_f \sin\vartheta_i \end{aligned} \tag{1.70}$$

Under isotropic conditions, the *a priori probability* for a certain orientation is given by the solid-angle ratio

$$p(\vec{u}_i)\ \sin\vartheta_i\, \mathrm{d}\vartheta_i\, \mathrm{d}\varphi_i = \frac{\mathrm{d}\Omega_i}{4\pi} = \frac{1}{4\pi}\ \sin\vartheta_i\, \mathrm{d}\vartheta_i\, \mathrm{d}\varphi_i \tag{1.71}$$

Inserting this in eqn (1.70) gives the expression to be evaluated:

$$\mathcal{G}_k(\tau) = (-1)^k \int_0^{2\pi} \mathrm{d}\varphi_f \int_0^{\pi} \mathrm{d}\vartheta_f \int_0^{2\pi} \mathrm{d}\varphi_i \int_0^{\pi} \mathrm{d}\vartheta_i P_c\left(\vec{u}_i, \vec{u}_f, \tau\right) Y_{2,k}(\vec{u}_i) Y_{2,-k}\left(\vec{u}_f\right) \sin\vartheta_f \sin\vartheta_i \tag{1.72}$$

The crucial term in eqn (1.72) is the conditional probability density $P_c(\vec{u}_i, \vec{u}_f, \tau)$. For continuous rotational diffusion, it will be a solution of the rotational variant of the diffusion equation[2,5]

$$\frac{\partial P_c(\vec{u}_i, \vec{u}_f, \tau)}{\partial \tau} = D_\mathrm{r} \nabla^2 P_c(\vec{u}_i, \vec{u}_f, \tau) \tag{1.73}$$

where D_r is the rotational diffusion coefficient and ∇^2 is the Laplace differential operator for polar coordinates r, φ, ϑ. With the Dirac delta function, the initial condition can be expressed as

$$P_c(\vec{u}_i, \vec{u}_f, 0) = \delta(\vec{u}_f - \vec{u}_i) \tag{1.74}$$

Expanding in terms of spherical harmonics, expressing the Laplace operator in spherical coordinates and exploiting the orthonormal properties of spherical harmonics leads – after some lengthy but straightforward calculus – to the monoexponential autocorrelation function

$$\mathcal{G}_k(\tau) = 4\pi(-1)^k \left\langle Y_{2,k}[\vec{u}(0)] Y_{2,-k}[\vec{u}(\tau)] \right\rangle = \exp(-|\tau|/\tau_\mathrm{rot}) \tag{1.75}$$

with the rotational correlation time $\tau_\mathrm{rot} = (6D_\mathrm{rot})^{-1}$ and the rotational diffusion coefficient D_rot.[5] Note that this result does not depend on the order k, as already stated by eqn (1.13).

Isotropic rotational diffusion is expected for spherical molecules such as certain globular proteins[39–41] and hydration complexes of paramagnetic ions[34–36] [see eqn (1.80)], and – to some extent – cyclohexane in the plastic phase,[42] for instance. Exponential correlation functions and hence Lorentzian spectral densities are also observed in cases where rotational diffusion is restricted to a fixed rotation axis within the time scale of spin–lattice relaxation. Examples are methyl side groups of amino acids and polypeptides[43] and benzene crystals.[44] Finally, simple two-site exchange processes as found in gypsum[26] also reveal exponential autocorrelation functions.

With less symmetric and more complex scenarios of molecular dynamics, autocorrelation decays can be far from monoexponential. Most applications reported in this book actually refer to complex systems. Examples are chain modes of polymers (see Figure 1.7b and Chapters 8 and 13), diffusion of adsorbate molecules along adsorbent surfaces (see Figure 1.7c and Chapters 9, 12, 18, 19 and 20) and order director fluctuations in liquid crystals[5] (see Figure 1.7d and Chapter 11).

A more general approach to formulate correlation functions is to interpret them as probabilities that the dynamic processes in question have *not yet* taken place after an interval τ. Usually, the complementary probability is primarily available, namely the probability $W(\tau)$ that the corresponding process has occurred. The (normalized) correlation function is then

$$\mathcal{G}(\tau) \approx 1 - W(\tau) \tag{1.76}$$

Examples of such treatments can be found in ref. 45 for polymer segment reorientation by reptation and in ref. 14 and 15 for defect diffusion models in solid-like or ordered structures. In the case of reptation of polymer chains in a fictitious tube, the autocorrelation function for segment reorientation is identified with the probability that the polymer segment is still (or again) at the same position of the tube after the interval τ, and has not yet diffused away. That is, the tube is supposed to determine the segment orientation on the time scale relevant for reptation. Likewise, translational diffusion of structural (reorienting or structurally dilating) defects means that local spin couplings in molecules or molecular groups can only fluctuate subject to the arrival of such defects. The autocorrelation function is then the probability that no such defects have arrived during τ. Note that molecular fluctuations are the consequence of *translational* displacements in these particular model concepts.

One last remark with regard to autocorrelation functions: there may be a distribution of relaxation times (or functions) in heterogeneous systems if exchange is slow enough, as discussed in Section 1.2.1.2. However, for a single monoexponential relaxation scenario (*i.e.* for fast exchange on the relaxation time scale), there is strictly no such thing as a *distribution of correlation functions*. All molecular dynamics occurring on the time scale of spin–lattice relaxation, $\tau \leq T_1$, is to be represented by a single autocorrelation function, potentially implying a *distribution of components* with different local correlation and exchange time constants. We will return to this subject in the next section.

1.3.2 Parallelism of Correlation and Relaxation Functions

Regarding eqn (1.14)–(1.17), (1.21), (1.26) and (1.27), one finds that all these expressions for spin–lattice relaxation rates are linear combinations of (normalized) spectral densities for intramolecular interactions and (unnormalized) spectral densities for intermolecular couplings:

$$\frac{1}{T_1} = \sum_{k=0,1,2} \left[a_k \mathcal{J}(\omega_k) + b_k \mathcal{J}_k^{\text{inter}}(\omega_k) \right] \tag{1.77}$$

Weighted with coefficients a_k and b_k, spectral densities for zero-, single- and double-quantum transitions are simply added up as far as relevant. Intra- and intermolecular relaxation rates are plainly added [see eqn (1.17)]. Relaxation in multi-spin systems is approached by sums of two-spin terms [see eqn (1.16)]. This analytical simplicity may be the reason why most researchers prefer to plot dispersions of relaxation *rates* rather than relaxation *times*.

Zero-, single- and double-quantum transitions and intra- and intermolecular interactions are *independent* sources of relaxation. According to eqn (1.77), the effective relaxation function [see eqn (1.37)] is therefore a product of the individual relaxation contributions:

$$\frac{M_z(\tau) - M_0(B_\text{r})}{M_0(B_\text{p}) - M_0(B_\text{r})} = \prod_{k=0,1,2} \left[\text{e}^{-a_k \mathcal{J}(\omega_k)\tau} \text{e}^{-b_k \mathcal{J}_k^{\text{inter}}(\omega_k)\tau} \right] \tag{1.78}$$

There is a certain parallelism between relaxation and correlation functions provided that correlation functions are monoexponential: Let us label the correlation loss rates $1/\tau_m$ for superimposed stochastic processes labelled with the subscript m. The analogue to eqn (1.78) for the effective correlation function is then

$$\mathcal{G}(\tau) = \prod_m \exp\left(-\frac{|\tau|}{\tau_m} \right) \tag{1.79}$$

A well-known example is proton spin–lattice relaxation in aqueous solutions of electron paramagnetic ions, where dipolar couplings with the spins of the unpaired electrons dominate.[35,36] Dipolar interactions fluctuate owing to rotational diffusion of the ion hydration complex (correlation time τ_rot), by electron spin flips (correlation time*** τ_S) and by exchange between hydration shells and bulk solvent (correlation time τ_des). The individual correlation functions of all these processes are monoexponential. In total, this leads to the autocorrelation function

$$\mathcal{G}(\tau) = \exp\left(-\frac{|\tau|}{\tau_\text{rot}} \right) \exp\left(-\frac{|\tau|}{\tau_S} \right) \exp\left(-\frac{|\tau|}{\tau_\text{des}} \right) = \exp\left(-\frac{|\tau|}{\tau_\text{c}} \right) \tag{1.80}$$

***From the point of view of electron spin resonance, τ_S is actually a relaxation time.

with the correlation loss rate

$$\frac{1}{\tau_c} = \frac{1}{\tau_{rot}} + \frac{1}{\tau_S} + \frac{1}{\tau_{des}} \tag{1.81}$$

Eqn (1.80) is the probability that none of the three processes has taken place in the interval τ.

One is tempted to extend this additive property generally to the superposition of different dynamic processes. Take, for instance, a nematic liquid crystal domain, in which molecules on the one hand rotate about their long axes and on the other are independently subjected to collective order-director fluctuations.[5] Let the correlation functions of the respective components be $\mathcal{G}^{(rot)}(\tau)$ and $\mathcal{G}^{(ODF)}(\tau)$. The probability considerations outlined in the previous section suggest that the correlation function $\mathcal{G}(\tau)$ of superimposed, stochastically independent molecular dynamics fluctuations results as the *product* of their component correlation functions, *i.e.*

$$\mathcal{G}(\tau) = \mathcal{G}^{rot}(\tau)\mathcal{G}^{(ODF)}(\tau) \tag{1.82}$$

The Fourier transform of this product is definitely not a sum or linear combination of the component spectral densities. However, under certain conditions the resulting relaxation rate can nevertheless be *approached* by a linear combination. This will be pointed out in the following section.

1.3.3 Superposition of Restricted Fluctuations

The three types fluctuations assumed in eqn (1.80) are characterized by different correlation loss rates. However, they are all assumed to be *unrestricted*, so that no constraints with respect to molecular orientations or electron spin state are effective. In contrast, superpositions of different fluctuation processes are of particular interest if molecular motions are partially or entirely subject to steric or microstructural constraints. Such *restricted fluctuations* are characterized by correlation functions of the type

$$\mathcal{G}(\tau) = g(\tau) + \mathcal{G}(\infty) \tag{1.83}$$

where $g(\infty) = 0$ and $\mathcal{G}(\infty)$ is a finite constant, that is, the function does not decay to zero but rather leaves a residual correlation $\mathcal{G}(\infty)$ in the long-time limit.

Typical examples for such superpositions of more or less restricted fluctuations are (i) rotational diffusion *versus* order-director fluctuations in *liquid crystals* (as already mentioned), (ii) local *polymer segment* reorientations *versus* global chain modes, (iii) rotational diffusion of *side groups* of proteins *versus* tumbling of the whole macromolecule and (iv) rotational diffusion of adsorbate molecules in porous or colloidal media *versus* surface diffusion (*i.e.* the RMTD process referred to in Sections 1.1.1.3 and 1.2.2.6).

Assume, for instance, a stochastically independent superposition of fast restricted and slow unrestricted components. The effective correlation

function then consists of the *product* of the correlation functions of the two components:

$$\mathcal{G}(\tau) = \underbrace{\mathcal{G}^{(\mathrm{f,r})}(\tau)}_{\text{fast restricted}} \qquad \underbrace{\mathcal{G}^{(\mathrm{s,u})}(\tau)}_{\text{slow unrestricted}} \tag{1.84}$$

where the superscripts f,r and s,u stand for 'fast and restricted' and 'slow and unrestricted', respectively. The corresponding correlation times [in the sense of eqn (1.5)] are assumed to be related as $\tau_c^{(\mathrm{s,u})} \gg \tau_c^{(\mathrm{f,r})}$. The reorientational restriction manifests itself by a finite residual correlation for the fast restricted process:

$$\mathcal{G}^{(\mathrm{f,r})}(\tau) = g^{(\mathrm{f,r})}(\tau) + \mathcal{G}^{(\mathrm{f,r})}(\tau \to \infty) \tag{1.85}$$

where $g^{(\mathrm{f,r})}(\tau \to \infty) = 0$ and $\mathcal{G}^{(\mathrm{f,r})}(\tau \to \infty) = \text{constant} \equiv A$. Inserting eqn (1.85) in eqn (1.84) gives

$$\begin{aligned} \mathcal{G}(\tau) &= \left[g^{(\mathrm{f,r})}(\tau) + A\right]\mathcal{G}^{(\mathrm{s,u})}(\tau) \\ &= g^{(\mathrm{f,r})}(\tau)\mathcal{G}^{(\mathrm{s,u})}(\tau) + A\mathcal{G}^{(\mathrm{s,u})}(\tau) \end{aligned} \tag{1.86}$$

On the time scale $\tau \ll \tau_c^{(\mathrm{s,u})}$, *i.e.* where $g^{(\mathrm{f,r})}(\tau)$ is still finite, the component for slow unrestricted reorientations can be set as $\mathcal{G}^{(\mathrm{s,u})}(\tau \ll \tau_c^{(\mathrm{s,u})}) \approx 1$. According to this *different time-scale approach*, the total autocorrelation function eqn (1.86) is reduced to

$$\mathcal{G}(\tau) \approx g^{(\mathrm{f,r})}(\tau) + A\mathcal{G}^{(\mathrm{s,u})}(\tau) \tag{1.87}$$

In this approximation, we have a sum expression indeed, and the spectral density obeys

$$\mathcal{J}(\omega) \approx \mathcal{J}^{(\mathrm{f,r})}(\omega) + A\mathcal{J}^{(\mathrm{s,u})}(\omega) \tag{1.88}$$

The corresponding spin–lattice relaxation rate is

$$\frac{1}{T_1} \approx \sum_{k=0,1,2} a_k \left[\mathcal{J}^{(\mathrm{f,r})}(\omega_k) + A\mathcal{J}^{(\mathrm{s,u})}(\omega_k)\right] \quad \text{for} \quad \tau_c^{(\mathrm{s,u})} \gg \tau_c^{(\mathrm{f,r})} \tag{1.89}$$

Figure 1.7b–d illustrate a number of model scenarios for which such superpositions of fast restricted and slow restricted or unrestricted processes can be expected.

A further class of systems characterized by restricted fluctuations is *liquid crystals*. In this context, we have already postulated eqn (1.82) as an example for superposition of two stochastically independent restricted fluctuation components. The expression given there can be expanded according to

$$\begin{aligned} \mathcal{G}(\tau) &= \mathcal{G}^{(\mathrm{rot})}(\tau)\mathcal{G}^{(\mathrm{ODF})}(\tau) \\ &= \left[g^{(\mathrm{rot})}(\tau) + \mathcal{G}^{(\mathrm{rot})}(\infty)\right]\left[g^{(\mathrm{ODF})}(\tau) + \mathcal{G}^{(\mathrm{ODF})}(\infty)\right] \end{aligned} \tag{1.90}$$

where $g^{(\mathrm{rot})}(\infty) = 0$, $g^{(\mathrm{ODF})}(\infty) = 0$, $\mathcal{G}^{(\mathrm{rot})}(\infty) = \text{constant}$ and $\mathcal{G}^{(\mathrm{ODF})}(\infty) = \text{constant}$. If the correlation times of the components are very different – for

the present case, *e.g.* $\tau_{\mathrm{rot}} \ll \tau_{\mathrm{ODF}}$ – eqn (1.90) can be approached by a linear combination

$$\begin{aligned} \mathscr{G}(\tau) &= \left[g^{(\mathrm{rot})}(\tau) + \mathscr{G}^{(\mathrm{rot})}(\infty)\right]\left[g^{(\mathrm{ODF})}(\tau) + \mathscr{G}^{(\mathrm{ODF})}(\infty)\right] \\ &\approx a g^{(\mathrm{rot})}(\tau) + b g^{(\mathrm{ODF})}(\tau) + c \end{aligned} \tag{1.91}$$

where a, b and c are constants resulting from multiplying out the binomial brackets and applying the relevant approximations for the mixed terms in the short- and long-time limits $\tau \ll \tau_{\mathrm{ODF}}$ and $\tau \gg \tau_{\mathrm{rot}}$, respectively. Under the above conditions, the spin–lattice relaxation rate can then be approached by $1/T_1 \approx [a/T_1^{(\mathrm{rot})}] + [b/T_1^{(\mathrm{ODF})}]$.

Taken together, the *necessary* conditions permitting one to approximate correlation functions of superimposed fluctuation components,

$$\mathscr{G}(\tau) \approx a_0 + a_1 g_1(\tau) + a_2 g_2(\tau) + \cdots \tag{1.92}$$

and the corresponding spin–lattice relaxation rate,

$$\frac{1}{T_1} \approx \frac{a_1}{T_1^{(1)}} + \frac{a_2}{T_1^{(2)}} + \cdots \tag{1.93}$$

by linear combinations are (i) the fluctuation components must be *stochastically independent*, (ii) the fluctuation components must be spatially *restricted* in general, but one of them may be unrestricted, and (iii) the correlation times of the components must substantially *differ* from each other, the more the better.

1.4 Concluding Remarks

In this chapter, we have outlined the framework conditions of field-cycling NMR relaxometry. These include (i) technical specifications required for successful field-cycling experiments, (ii) physical limits and (iii) the relevant theoretical background, interpretation standards and elements of the calculus of autocorrelation functions and spectral densities. The following 20 chapters delineate a wealth of knowledge concerning solutions of instrumental problems, applications in the full range of accessibility by the technique and the explanatory power of theoretical model treatments. In this sense, the present book may serve as a source of inspiration for the interested reader who is looking forward to carrying out innovative field-cycling studies.

References

1. C. V. Heer, *Statistical Mechanics, Kinetic Theory, and Stochastic Processes*, Academic Press, New York, 1972.

2. A. Abragam, *The Principles of Nuclear Magnetism*, Clarendon Press, Oxford, 1961.
3. C. P. Slichter, *Principles of Magnetic Resonance*, Springer, Berlin, 1990.
4. D. Kruk, *Theory of Evolution and Relaxation of Multi-Spin Systems*, Arima Publishing, Bury St. Edmunds, 2007.
5. R. Kimmich, *Principles of Soft-Matter Dynamics*, Springer, Dordrecht, 2012.
6. U. Haeberlen, *High Resolution NMR in Solids*, Academic Press, New York, 1976.
7. R. Kimmich, *NMR: Tomography, Diffusometry, Relaxometry*, Springer, Berlin, 1997.
8. L. G. Werbelow and D. M. Grant, *Adv. Magn. Reson.*, 1977, **9**, 189.
9. A. Kumar, R. C. R. Grace and P. K. Madhu, *Prog. Nucl. Magn. Reson. Spectrosc.*, 2000, **37**, 191.
10. P. A. Beckmann and A. I. Rheingold, *J. Chem. Phys.*, 2016, **144**, 154308.
11. P. S. Hubbard, *J. Chem. Phys.*, 1970, **52**, 563.
12. R. Kimmich and N. Fatkullin, *Prog. Nucl. Magn. Reson. Spectrosc.*, 2017, **101**, 18.
13. S. Stapf, R. Kimmich and R.-O. Seitter, *Phys. Rev. Lett.*, 1995, **75**, 2855.
14. R. Kimmich and G. Voigt, *Z. Naturforsch. A*, 1978, **33**, 1294.
15. W. Nusser, R. Kimmich and F. Winter, *J. Phys. Chem.*, 1988, **92**, 6808.
16. W. Nusser and R. Kimmich, *J. Phys. Chem.*, 1990, **94**, 5637.
17. E. Anoardo, F. Grinberg, M. Vilfan and R. Kimmich, *Chem. Phys.*, 2004, **297**, 99.
18. R. Kimmich and N. Fatkullin, *Adv. Polym. Sci.*, 2004, **170**, 1.
19. J. Kärger, H. Pfeifer and W. Heink, *Adv. Magn. Reson.*, 1988, **12**, 1.
20. W. S. Price, *Concepts Magn. Reson.*, 1997, **9**, 299.
21. R. Orbach, *Science*, 1986, **231**, 814.
22. R. Kimmich, *Bull. Magn. Reson.*, 1980, **1**, 195.
23. F. Noack, *Prog. Nucl. Magn. Reson. Spectrosc.*, 1986, **18**, 171.
24. R. Kimmich and E. Anoardo, *Progr. Nucl. Magn. Reson. Spectrosc.*, 2004, **44**, 257.
25. F. Fujara, D. Kruk and F. Privalov, *Progr. NMR Spectroscopy*, 2014, **82**, 39.
26. D. C. Look and I. J. Lowe, *J. Chem. Phys.*, 1966, **44**, 2995.
27. B. A. Cornell and J. M. Pope, *J. Magn. Reson.*, 1974, **16**, 172.
28. R. Kimmich, J. Barenz and J. Weis, *J. Magn. Reson., Ser. A*, 1995, **117**, 228.
29. E. Anoardo, C. Hauser and R. Kimmich, *J. Magn. Reson.*, 2000, **142**, 372.
30. D. P. Weitekamp, A. Bielecki, D. Zax, K. Zilm and A. Pines, *Phys. Rev. Lett.*, 1983, **50**, 1807.
31. G. E. Pake, T. L. Estle, *The Physical Principles of Electron Paramagnetic Resonance*, Benjamin, Reading, 1973.
32. B. F. Melton, V. L. Pollak, T. W. Mayers and B. L. Willis, *J. Magn. Reson., Ser. A*, 1995, **117**, 164.
33. C. Mattea, R. Kimmich, I. Ardelean, S. Wonorahardjo and G. Farrher, *J. Chem. Phys.*, 2004, **121**, 10648.
34. R. Hausser and F. Noack, *Z. Phys.*, 1964, **182**, 93.

35. J. Kowalewski, L. Mäler, *Nuclear Spin Relaxation in Liquids*, Taylor and Francis, London, 2006.
36. I. Bertini, C. Luchinat, G. Parigi, *Solution NMR of Paramagnetic Molecules*, Elsevier, Amsterdam, 2001.
37. T. Zavada and R. Kimmich, *J. Chem. Phys.*, 1998, **109**, 6929.
38. R. Valiullin, R. Kimmich and N. Fatkullin, *Phys. Rev. E*, 1997, **56**, 4371.
39. S. H. Koenig and W. E. Schillinger, *J. Biol. Chem.*, 1969, **244**, 3283.
40. B. Blicharska, Z. Florkowski, J. W. Hennel, G. Held and F. Noack, *Biochim. Biophys. Acta*, 1970, **207**, 381.
41. R. Kimmich and F. Noack, *Ber. Bunsen-Ges. Phys. Chem.*, 1971, **75**, 269.
42. S. Stapf and R. Kimmich, *Mol. Phys.*, 1997, **92**, 1051.
43. E. R. Andrew, R. Gaspar, T. J. Green and W. Vennart, *Biopolymers*, 1978, **17**, 1913.
44. U. Haeberlen and G. Maier, *Z. Naturforsch. A*, 1967, **22**, 1236.
45. P. G. de Gennes, *J. Chem. Phys.*, 1971, **55**, 572.